

1 **Reanalysis of the longest mass balance series in Himalaya using a nonlinear model:**
2 **Chhota Shigri Glacier (India)**

3 Mohd. Farooq Azam¹, Christian Vincent², Smriti Srivastava^{1,3}, Etienne Berthier⁴, Patrick Wagnon²,
4 Himanshu Kaushik¹, Arif Hussain¹, Manoj Kumar Munda¹, Arindan Mandal⁵, and Alagappan
5 Ramanathan⁶

6 ¹Department of Civil Engineering, Indian Institute of Technology Indore, Simrol, India-453552

7 ²Univ. Grenoble Alpes, IRD, CNRS, INRAE, Grenoble INP, IGE, F-38000 Grenoble, France

8 ³Department of Geography, University of Utah, Salt Lake City, USA

9 ⁴Université de Toulouse, LEGOS (CNES/CNRS/IRD/UT3), Toulouse, 31400, France

10 ⁵Interdisciplinary Centre for Water Research, Indian Institute of Science, Bengaluru 560012, India

11 ⁶School of Environmental Sciences, Jawaharlal Nehru University, New Delhi-110067, India

12

13 Correspondence to: Mohd. Farooq Azam (farooqazam@iiti.ac.in; farooqaman@yahoo.co.in)

14 **Abstract**

15 The glacier-wide mass balance (MB) series on Chhota Shigri Glacier has been reanalysed by
16 combining the traditional MB reanalysis framework and a nonlinear MB model. The
17 nonlinear model is preferred over the traditional glaciological method to compute the
18 glacier-wide MBs as the former can capture the spatiotemporal variability of point MBs from
19 a heterogeneous in-situ point MB network. Further, the nonlinear model is also used to detect
20 erroneous measurements from the point MB observations over 2002–2023. ASTER and
21 Pléiades stereo-imagery show limited areal changes but negative mass balances of $-0.38 \pm$
22 0.05 m w.e. a^{-1} during 2003–2014 and -0.51 ± 0.06 m w.e. a^{-1} during 2014–2020. The
23 nonlinear model outperforms the traditional glaciological method and agrees better with these
24 geodetic estimates. The reanalysed mean glacier-wide MB over 2002–2023 is -0.47 ± 0.19 m
25 w.e. a^{-1} , equivalent to a cumulative loss of -9.81 ± 0.87 m w.e. Our analysis suggests that
26 the nonlinear model can also be used to complete the MB series if for some years the field
27 observations are poor or unavailable. With this analysis, we revisit the glacier-wide MB
28 series of Chhota Shigri Glacier and provide the most accurate and up-to-date version of this
29 series, the longest continuous ever recorded in the Himalaya. We recommend applying the
30 nonlinear model on all traditional glaciological mass balance series worldwide whenever data
31 is sufficient, especially in the Himalaya where in-situ data are often missing due to access
32 issues.

33

34

35

36 1. Introduction

37 Glaciers are excellent indicators of changing climate; therefore, long-term glacier mass
38 changes are observed to understand the impacts of climate change (Oerlemans, 2001; Zemp
39 et al., 2019). Glacier monitoring is also essential to understand possible glacial hazards
40 (Harrison et al., 2018; Shukla et al., 2018; Shugar et al., 2021; Gantayat and Ramsankaran,
41 2023), regional hydrology (Azam et al., 2021; Yao et al., 2022; Nepal et al., 2023), and sea
42 level rise (Gardner et al., 2013; Rounce et al., 2023). The glacier mass balance (MB) can be
43 estimated from satellite data, through modelling approaches or measured using the field-
44 based traditional glaciological method (Cogley, 2009; Zemp et al., 2015; Kumar et al., 2018;
45 Miles et al., 2021; Berthier et al., 2023).

46 Over the last decade, rapid development has been made through satellite geodetic MB
47 estimates covering almost all glacierized areas in the Himalaya (Brun et al., 2017; Bolch et
48 al., 2019; Shean et al., 2020; Hugonnet et al., 2021; Jackson et al., 2023). These geodetic
49 estimates are primarily available at a multiannual scale and thus cannot be used to study the
50 inter-annual variability in glacier MB. Conversely, field measurements using standard
51 methods (Østrem and Stanley, 1969) yield data on the seasonal/annual response of glacier
52 MB to local meteorological conditions (Zemp et al., 2015). Field MB observations remain
53 scarce in the Himalaya compared to the other mountain ranges (Azam et al., 2018) and have
54 been limited to only 35 glaciers (Vishwakarma et al., 2022). Most observations are available
55 from easily accessible and small glaciers for short periods, generally less than 10-15 years.
56 The ongoing MB series include Chhota Shigri, Hoksar, Kolahoi and Sutri Dhaka glaciers in
57 the western Himalaya (Oulkar et al., 2022; Mandal et al., 2020; Romshoo et al., 2022; 2023),
58 Mera, Pokalde, Rikha Samba, Trambau, West Changri Nup, Yala glaciers in the central
59 Himalaya (Sunako et al., 2019; Wagnon et al., 2021; Stumm et al., 2021), and Ganju La and
60 Thana glaciers in the eastern Himalaya (Tshering and Fujita, 2016).

61 For annual glacier-wide MB estimation, the traditional glaciological method has been
62 used in the Himalaya (Azam et al., 2018). This method involves interpolation/extrapolation
63 of point MB measurements from fixed locations to the whole glacier area by applying
64 different approaches, including contouring, profiling, and kriging (Østrem and Brugman,
65 1991; Zemp et al., 2013) or application of observed MB gradients to the glacier hypsometry
66 (Funk et al., 1997; Wagnon et al., 2021). The selected point measurement sites may not be
67 representative of the surrounding areas because (1) ablation stakes are often inserted away
68 from the steep slopes towards the valley walls for safety reasons; thus, snow avalanche inputs

69 onto valley glaciers are not included; (2) crevassed areas are not sampled, (3) snow
70 accumulation is site-specific and largely depends on local topography that controls snow drift
71 and deposition and (4) harsh weather sometimes restricts access to accumulation
72 measurement sites. Almost all the MB series are victims of one or other such issues;
73 therefore, the estimated glacier-wide MBs often carry systematic biases (Thibert et al., 2008).
74 These biases can be corrected by calibrating the MB series using satellite-derived geodetic
75 mass estimates generally over 5-10 years (Zemp et al., 2013; Wagnon et al., 2021).

76 Furthermore, it is practically difficult to keep the position fixed for point
77 measurements due to accessibility issues, stake displacement due to glacier dynamics, use of
78 different surveying equipment (GPS, dGPS, total station, theodolite, etc.) and different
79 researchers' involvement for decades of monitoring. Hence, the measurement network differs
80 in space and time. In this situation, heterogeneous in-situ measurements do not always allow
81 to catch the large spatiotemporal variability of point MBs within the same elevation range
82 (Funk et al., 1997; Vincent and Six, 2013); consequently, the point MB-elevation relationship
83 is insufficient to investigate the changes in glacier-wide MBs (Kuhn, 1984; Huss and Bauder,
84 2009; Thibert et al., 2013).

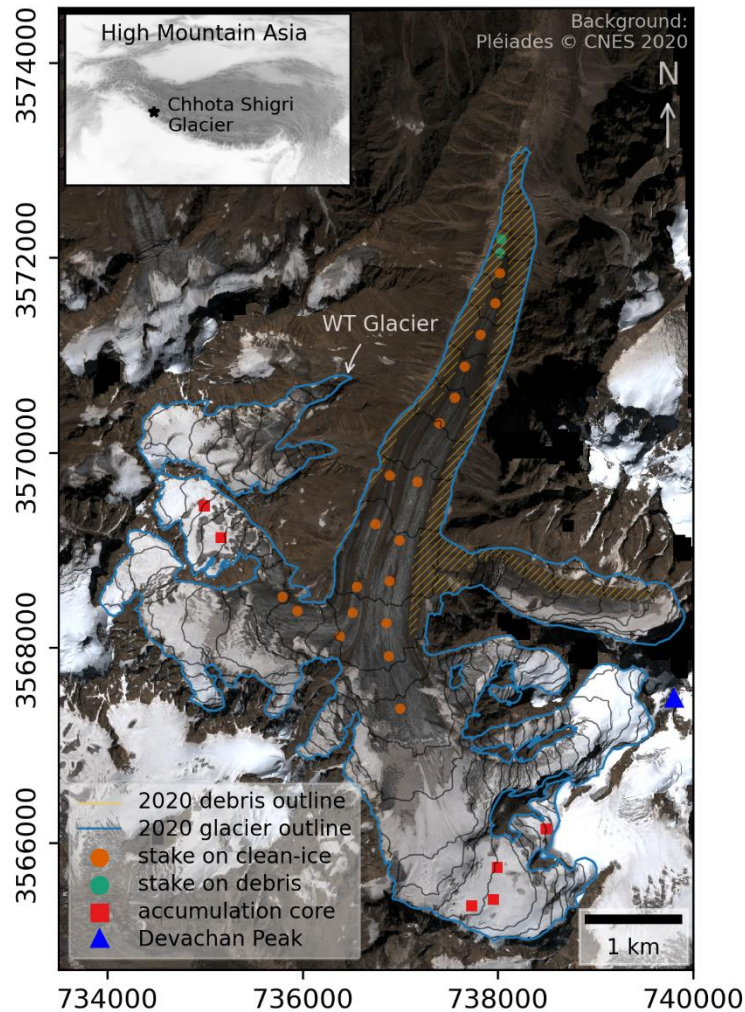
85 To include the spatiotemporal variability of point MB measurements, Lliboutry
86 (1974) proposed a linear statistical model and tested it over the small ablation area of Saint
87 Sorlin Glacier (France), assuming similar temporal changes of the MB over the whole area.
88 Vincent et al. (2018) suggested that the linear model of Lliboutry (1974) was valid over a
89 limited elevation range but ignored the decreasing spatiotemporal variability of point MBs
90 with elevation (Oerlemans, 2001). To address this issue, they proposed a nonlinear model that
91 considers the decreasing spatiotemporal changes in point MBs over the large elevation range
92 and successfully tested their model on four different glaciers from different climate regimes,
93 including Chhota Shigri Glacier (India).

94 The MBs on Chhota Shigri Glacier were estimated using the nonlinear model over
95 2002–2016 and then calibrated using geodetic MB over 2005–2014 (Vincent et al., 2018). In
96 the present study, we extended the MB series on Chhota Shigri Glacier up to 2023 using the
97 traditional method, estimated the areal changes and geodetic MBs over the 2003–2014 and
98 2014–2020 periods, estimated the debris cover as of September 2020, and reanalysed the
99 annual MB series since 2002 using a novel reanalysis framework that combines the Vincent
100 et al. (2018) nonlinear model and the reanalysis framework proposed by Zemp et al. (2013).
101 Additionally, we assessed areal changes and geodetic MBs of neighbouring glaciers Hamtah
102 and Sichum over the same periods based on available satellite stereo-images.

103 Since 2002, the MB series of Chhota Shigri Glacier has been continuously monitored,
104 making it the longest series in the Himalaya. Azam (2021) highlighted the importance of
105 Chhota Shigri as a reference glacier for large-scale MB and hydrological studies; therefore,
106 the main aim of the present study is to produce the most accurate glacier-wide MB series in
107 this region. First, the nonlinear model of Vincent et al. (2018) was used to detect the
108 erroneous point MB measurements in the dataset. Second, the nonlinear model was applied
109 using the observed point MBs to estimate the glacier-wide MB at an annual scale. Third,
110 homogenization of the glacier-wide MB series accounting for glacier areal changes was
111 performed; and fourth, the glacier-wide MB series was calibrated using geodetic MBs.
112 Additionally, we compared the performance of the nonlinear model with the traditional
113 method for estimating glacier-wide MB. We also assessed the nonlinear model's ability to
114 estimate glacier-wide MB using end-of-season snowline data when field measurements were
115 unavailable in a particular year.

116 2. Study area

117 Chhota Shigri Glacier (32.28° N, 77.58° E) is in the Chandra River Basin, a tributary of
118 Upper Indus Basin, Lahaul-Spiti valley of the western Himalaya (Fig. 1). Chhota Shigri flows
119 from 5830 to 4100 m a.s.l., with a length of ~9 km and an area of 15.47 km² (in 2020). Based
120 on the most updated map obtained in September 2020, 12% of its total surface area is covered
121 with debris between the snout and 4500 m a.s.l., including medial and lateral moraines from
122 4100 to ~4900 m a.s.l. and a debris-covered eastern tributary glacier (Fig. 1). Debris
123 thickness ranges from less than a few centimetres of thin debris to a few meters of boulders.
124 Valley walls bound its accumulation area, with the highest Devachan peak (6250 m a.s.l.).
125 The accumulation area has two east- and west-oriented tributaries that feed to the main
126 ablation area (<5070 m a.s.l.), having a north aspect and divided into two parallel flows by a
127 medial moraine.



128

129 **Figure 1:** Chhota Shigri Glacier showing the location of ablation and accumulation point
 130 measurement sites. Orange strips show the debris-covered glacier area. The background
 131 image is a Pléiades satellite image taken on 12 September 2020 (Copyright CNES 2020,
 132 Distribution Airbus Defence and Space). The glacier extent corresponds to 12 September
 133 2020. The coordinates are in UTM North, Zone 43.

134

135 Chhota Shigri is a well-studied glacier for various aspects, including traditional MBs,
 136 energy balance, dynamics, ice thickness, hydrology, etc. (Wagnon et al., 2007; Azam et al.,
 137 2012; Ramsankaran et al., 2018; Haq et al., 2021; Srivastava and Azam, 2022a; Mandal et al.,
 138 2020, 2022). Several studies have also observed its geodetic MBs (Berthier et al., 2007;
 139 Vincent et al., 2013; Brun et al., 2017; Mukherjee et al., 2018). Long-term annual MBs have
 140 been reconstructed over 1950–2020 applying a temperature index model (Srivastava et al.,
 141 2022) and over 1979–2020 using an energy balance model (Srivastava and Azam, 2022b).
 142 Due to recent glacier wastage on Chhota Shigri Glacier, the western tributary (WT) glacier
 143 got disconnected in the summer of 2012 (Srivastava et al., 2022). The fragmented tributary is
 144 now clearly visible in the high-resolution Pléiades image from 12 September 2020 (Fig. 1).

145 In this study, we focus on Chhota Shigri Glacier, but the available satellite stereo-
146 images also cover neighbouring Hamtah and Sichum glaciers; therefore, we also estimated
147 the areal changes and geodetic MBs for these two glaciers (sections 3.4 and 3.5). Hamtah
148 Glacier has been studied for its MBs and avalanche contribution (Vincent et al., 2013; Laha
149 et al., 2017). Further, for all three glaciers, we also delineated the debris cover corresponding
150 to 2020 (Table 1).

151 3. Methods

152 3.1 Traditional mass balance method

153 Glacier-wide annual MBs (B_a) have been estimated using a network of 22-25 ablation
154 bamboo stakes (inserted up to 10 m into the glacier) distributed over 4300-4900 m a.s.l. along
155 the main axis of the glacier (Fig. 1), and 4-6 accumulation pits/cores over 5160-5550 m a.s.l.
156 distributed over the eastern and western tributaries of the glacier (Wagnon et al., 2007). The
157 traditional glaciological profile method was used to estimate the glacier-wide MB from the
158 observed point MBs (Østrem and Stanley, 1969). First, using the observed point MBs, the
159 mean altitudinal MBs were estimated for each 50-m elevation band from available point MBs
160 within each elevation band (Fig. 1). In case no measurements were available (due to loss of
161 stakes or missing accumulation measurements) the MBs were estimated using linear
162 interpolation/extrapolation of neighbouring bands. Second, the B_a (in m w.e. a⁻¹) was
163 estimated as follows:

$$164 \quad B_a = \frac{1}{S} \sum_{z=min}^{z=max} b_z s_z, \quad (1)$$

165 where b_z is the mean altitudinal MB (in m w.e. a⁻¹) of a given elevation band, z , of area s_z
166 (m²) and S is the total glacier area (m²). In the ablation area, emergence changes at each
167 ablation stake were converted to the point MB using a fixed density of 900 kg m⁻³ for ice and
168 350 kg m⁻³ for snow (Wagnon et al., 2007; Cogley et al., 2011), while in the accumulation
169 area, the varying snow/firn/ice densities (350-900 kg m⁻³) were measured in the field. The
170 hydrological year for MB calculations is defined from 1 October to 30 September of the
171 following year; however, the exact measurement dates on site varied from a couple of days to
172 a week. Following Thibert et al. (2008), an overall uncertainty of ± 0.40 m w.e. a⁻¹ for
173 glacier-wide MB was estimated by incorporating the errors in point measurements and their
174 distribution over the glacier (Azam et al., 2012).

175 Due to access difficulties, snowstorms like on 22-24 September 2018, or logistical or
176 budget issues, **a limited number of point MB measurements could be carried out in some**
177 **years**. This was the case for October 2015, **when** only two accumulation measurements could
178 be performed, or 2018, **when** measurements were done early in the season, before the storm.
179 For those two years, point MB data in the accumulation zone, where no measurements had
180 been taken, was estimated using previous years with a similar ablation pattern (Mandal et al.,
181 2020). In 2020, only two in-situ point MB data are available, preventing the traditional
182 method from being applied. Further, no measurements could be performed in 2021; hence, no
183 MB could be estimated. Supplementary Table S1 provides all information about the point
184 MBs and field expeditions since 2002.

185 **3.2 Nonlinear mass balance model**

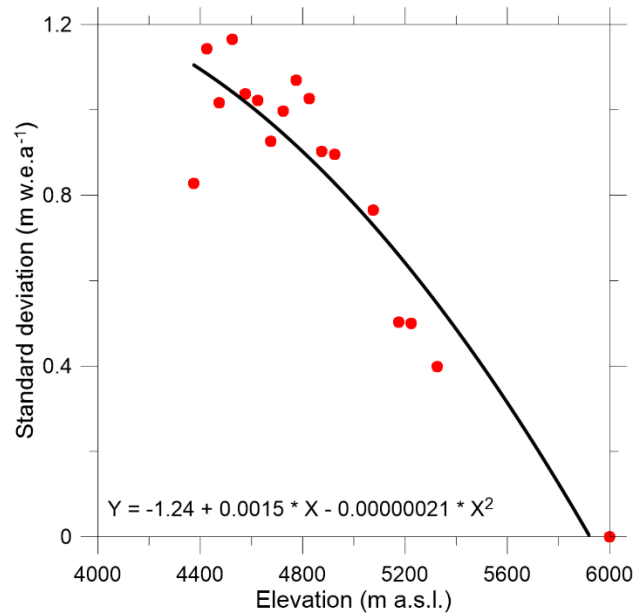
186 The nonlinear MB model suggests that the observed point MB, $b_{i,t}$, at any site i for year t , can
187 be decomposed into (1) **a spatial effect term, α_i** , and (2) **a temporal term, β_t** , combined with a
188 spatial effect, γ_i , and can be written as (Vincent et al., 2018):

$$189 \quad b_{i,t} = \alpha_i + \beta_t \gamma_i + \varepsilon_{i,t}, \quad (2)$$

190 where α_i , the spatial **effect** at location i , is the average point MB at the site over the whole
191 study period, β_t is the annual deviation from the average point MB (thus $\sum \beta_t = 0$), and $\gamma_i =$
192 σ_i/σ_{max} is a scaling factor defined as the ratio of the standard deviation of annual MB at site i
193 **and** the maximum standard deviation (σ_{max}) observed from the point MB measurements over
194 a long period. The $\varepsilon_{i,t}$ term represents residuals resulting from measurement errors and
195 inconsistencies between the model and observed data. The spatiotemporal decomposition
196 proposed in equation 2 assumes that β_t is the same at **all point locations** for any given year (t)
197 and thus has a glacier-wide significance while γ_i term accounts for nonlinear effects with
198 elevation (Vincent et al., 2018).

199 To compute the scaling factor, γ_i , on Chhota Shigri Glacier, standard deviations were
200 computed from the point MBs available for each 50-m elevation band as the point MBs are
201 not available each year from the same fixed locations (Fig. 2). The standard deviations were
202 computed only for 50-m elevation bands where mean annual MBs were available from in-situ
203 measurements over **a minimum of ten years**, and it was assumed that the computed standard
204 deviations are representative of the whole period of investigation (2002-2023). This resulted
205 in 16 standard deviation values over the whole glacier with a maximum standard deviation of
206 1.17 m w.e. a^{-1} at 4525 m a.s.l. (4500-4550 band) and a minimum standard deviation of 0.40

207 m w.e. a⁻¹ at 5325 m a.s.l. The decreasing magnitude of standard deviation with elevation
 208 indicates the decreasing sensitivity of the annual MB to temperature and precipitation (Fig.
 209 2), as already suggested by several studies on glaciers worldwide (Kuhn, 1984; Soruco et al.,
 210 2009; Basantes-Serrano et al., 2016; Vincent et al., 2018; Wagnon et al., 2021). The
 211 measurements are poor in the accumulation area, and no measurement was available above
 212 5325 m a.s.l.; therefore, after some trials, we adjusted the standard deviation at 6000 m a.s.l.
 213 to be zero (Fig. 2). A decreasing trend in standard deviation values below 4525 m a.s.l. (Fig.
 214 2) is due to the presence of debris cover over the tongue of Chhota Shigri Glacier (Fig. 1) that
 215 undermines the glacier's sensitivity to climate (Vincent et al., 2013; Banerjee and Shankar,
 216 2013). The scaling factor, γ_i , at each point MB location, was computed from the 2-degree
 217 polynomial function, fitted over the standard deviation vs elevation scatter plot (Fig. 2).



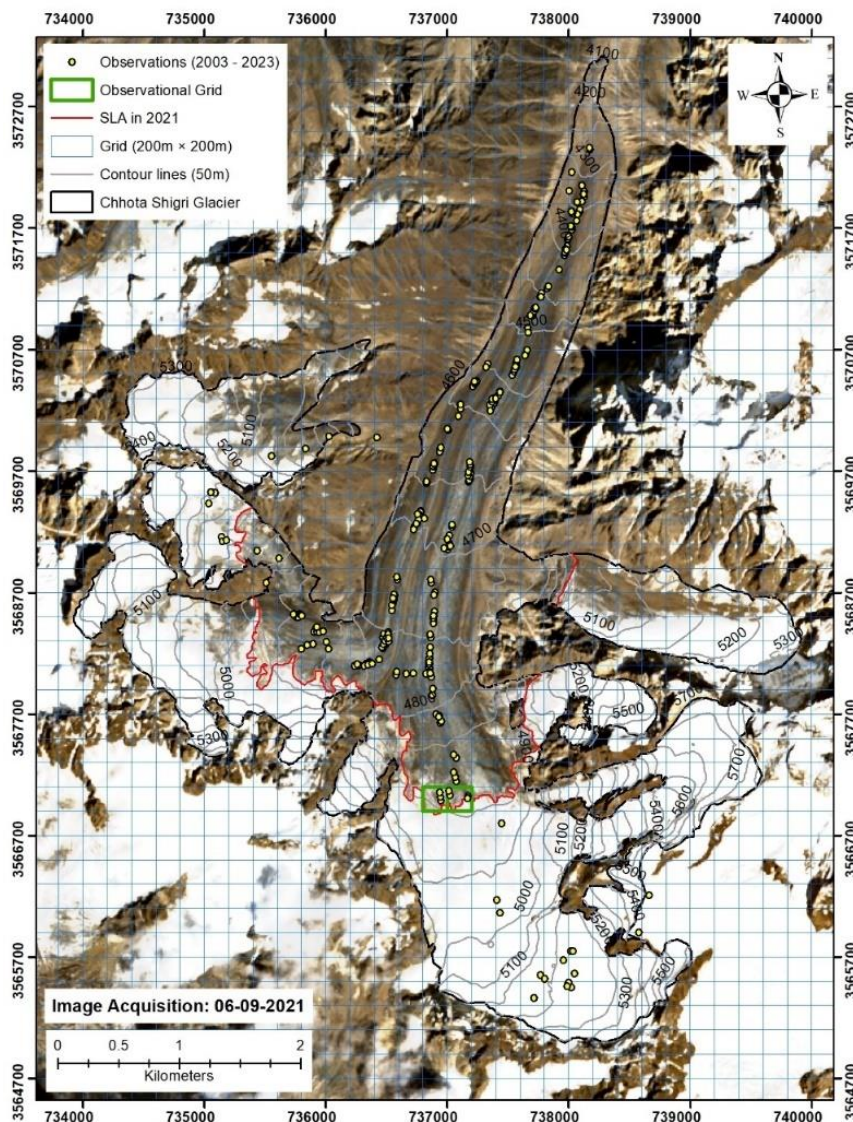
218

219 **Figure 2:** Standard deviations of the annual MBs versus elevation. The black line
 220 corresponds to a polynomial fit (degree of freedom = 2). The standard deviations were
 221 estimated for those 50m elevation bands where a minimum of 10 years of point
 222 measurements were available at each site, and it is assumed to be zero at 6000 m a.s.l. (above
 223 the glacier top at 5830 m a.s.l.).

224

225 The nonlinear model was run at 200m x 200m spatial resolution over 2002-2023
 226 using all available point MBs (413-point measurements, excluding the erroneous
 227 measurements, section 3.3) and polynomial equation (Fig. 2; details can be found in SI of
 228 Vincent et al., 2018). The MB is assumed to be spatially constant over each 200m x 200m
 229 grid for a given year. If there is more than one observation in a grid in a given year, then the
 230 mean MB of the available observations was used for MB computation. The grid size is a
 231 compromise between the spatial variability and the density of available point measurements.

232 Field measurements were unavailable in the 2020/21 year (section 3.1); hence, the
 233 nonlinear model cannot be run **for this hydrological year**. To run the model, at least one point
 234 MB measurement is required each year (Vincent et al., 2018). We assumed the snow line
 235 altitude (SLA) at the end of the ablation season to be equivalent to the equilibrium line
 236 altitude (ELA) (Rabatel et al., 2005; Brun et al, 2015; Davaze et al., 2020; Barandun et al.,
 237 2021). The SLA was delineated on a 6 September 2021 Sentinel image, and zero MBs (MB at
 238 ELA = 0 m w.e.) were assumed for two 200m x 200m grids where MB observations were
 239 available from other years (Fig. 3). It **should** be noted that there was no other cloud-free
 240 image from September 2021. The MB estimation from SLA using **the** nonlinear model is
 241 discussed in detail in section 5.3.



242

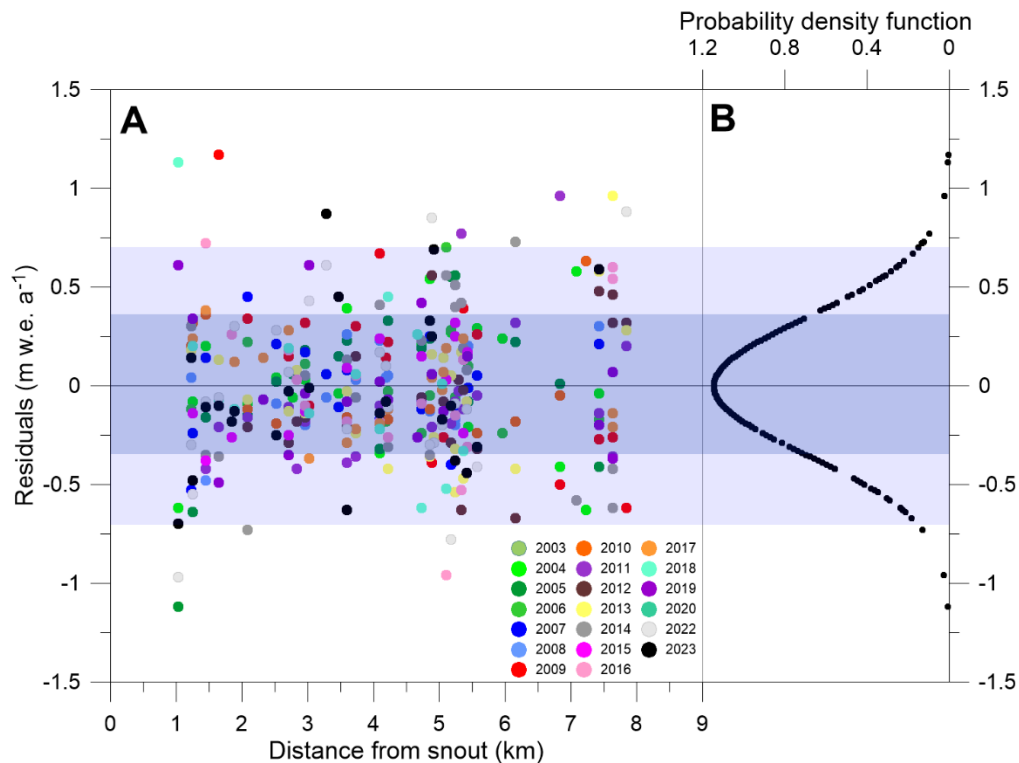
243 **Figure 3:** Distribution of all 413-point MB measurements (yellow dots) available over 2002-
 244 2023 on Chhota Shigri Glacier. The grids (in light blue) show a spatial resolution of 200m x

245 200m of the nonlinear model. For 2020/21, no field measurement was conducted; hence, two
246 grids (shown with green colour outline) corresponding to zero MB were selected on the
247 delineated SLA to run the model. The background is a Sentinel image from 6 September
248 2021, which is used to delineate the SLA.

249 The model output provides the mean α_i and mean γ_i for each point location over
250 2002–2023, and β_t for each year (equation 2). Fifty-four values for α_i and γ_i , and 21 values
251 for β_t (corresponding to each hydrological year) were computed (Table S2 and S3). For the
252 calculation of glacier-wide MB, a spatial distribution of α_i over the whole surface area of the
253 glacier is needed. First, for each 50-m elevation range (e), mean α_e was estimated from all
254 available α_i by taking a simple arithmetic mean and γ_e from all available γ_i from respective
255 elevation bands (equation 2). The modelled point MBs were available over the 4355–5512 m
256 a.s.l. elevation range and beyond this range, the mean α_e and γ_e from the lowest (4300–4350
257 m a.s.l.) and highest (5500–5550 m a.s.l.) ranges were used to cover the lowest (0.15 km²;
258 0.97% of total area) and highest (0.68 km²; 4.40% of total area) parts of the glacier. Second,
259 applying α_e , γ_e and β_t from all elevation bands in equation 1 along with corresponding
260 elevation areas, the annual glacier-wide MBs over 2002–2023 were estimated.

261 3.3 Tracking the erroneous in-situ point mass balances

262 The nonlinear model computes the residuals (difference between the measured and
263 theoretical values) of each measured point MB and can detect errors in in-situ point MB data
264 (Vincent et al., 2018). The distribution of residuals over the glacier as a function of distance
265 from the snout showed no spatio-temporal pattern (Fig. 4A), indicating that the nonlinear
266 model does not provide any apparent bias for any specific year. As expected, the residuals
267 followed a normal distribution with a standard deviation (STD) of 0.35 m w.e. a⁻¹ (Fig. 4B).
268 To detect the measurement errors in the point MBs in the Chhota Shigri measurement
269 network over 2002–2023, we assumed all the point MBs having residuals >2STD (0.70 m
270 w.e. a⁻¹) to be suspicious. Of 423-point MB measurements, 15 such point MBs were found
271 and investigated further. Five-point MBs had been wrongly reported from the notebooks and
272 thus have been corrected. We could not find any reason for the rest of the suspicious points.
273 Therefore, they have been considered erroneous and discarded in the final model run. The
274 erroneous data were collected in different years (five ablation point measurements from 2009,
275 2012, 2018 and 2022, and five accumulation point measurements from 2009, 2011, 2014 and
276 2022) (Fig. 4). The standard deviation of the residuals from the nonlinear model was reduced
277 from 0.35 to 0.30 m w.e. a⁻¹ after correction/removal of suspicious point MB measurements.



278

279 **Figure 4:** (A) Shows the residuals between measured and modelled point MBs from the
 280 nonlinear model using all available 423-point MBs as a function of distance from the glacier
 281 snout for each hydrological year between 2002 and 2023. The dark and light blue shaded
 282 envelopes represent the 1 STD and 2 STD values, respectively. (B) the probability density
 283 function (normal distribution curve) of all point MB residuals between 2002 and 2023.

284

285 3.4 Areal changes and debris cover estimation

286 The areal changes and debris cover were estimated on Chhota Shigri, Sichum and Hamtah
 287 glaciers by manual delineation following the Global Land Ice Measurements from Space
 288 (GLIMS) guidelines from the available ASTER (08/10/2003) and Pléiades images
 289 (26/09/2014 and 12/09/2020) (Raup et al., 2007). We have preferred manual delineation as it
 290 was considered the most accurate method for delineating glacier outlines (Stokes et al., 2007;
 291 Garg et al., 2017; Shukla and Qadir, 2016). The ice divides were interpreted using the
 292 Pléiades Digital Elevation model (DEM). The changes were estimated for the ablation area
 293 for 2014 and 2020, as the changes in the accumulation area were insignificant. The generated
 294 glacier outlines (2003, 2014 and 2020) were used to estimate the glacier area changes during
 295 2003–2020. The uncertainties associated with the glacier area were calculated using the
 296 buffer method (Bolch et al., 2010; Chand and Sharma, 2015). The buffer size was half the
 297 pixel value (Bolch et al., 2010; Andreassen et al., 2022).

298 3.5 Geodetic mass balances

299 The geodetic MBs were estimated over two periods (2003–2014 and 2014–2020) for Chhota
 300 Shigri, Sichum and Hamtah glaciers using satellite stereo images from ASTER (15 m
 301 resolution) acquired on 08/10/2003 and Pléiades (0.70 m resolution) acquired on 26/09/2014
 302 and 12/09/2020, respectively. The ASTER October 2003 stereo-pair was preferred to other
 303 ASTER or SPOT5 stereo pairs acquired in late summer 2002, 2004, and 2005 because it
 304 resulted in the smallest uncertainties. The stereo images were acquired close to the end of the
 305 hydrological year, reducing the impact of any seasonal offset. The DEM generation, co-
 306 registration and MB calculation procedure is the same as in Falaschi et al. (2023).
 307 Uncertainties for the glacier-wide geodetic MB were estimated using the patch method
 308 (Wagnon et al., 2021). **This method aims to empirically determine the uncertainty associated**
 309 **with the mean elevation change by sampling patches of stable terrain of various sizes to**
 310 **measure the decay of the error with the averaging area.**

311 Geodetic MBs were estimated over 10.97 years (from 08/10/2003 to 26/09/2014) and
 312 5.96 years (from 26/09/2014 to 12/09/2020) and linearly scaled to estimate the geodetic MBs
 313 over 11- and 6-year periods, respectively to make a direct comparison with the in-situ MBs
 314 (estimated from end of September to end of September next year). **Furthermore, the geodetic**
 315 **MBs included both the WT glacier, which fragmented around 2012 (Srivastava et al., 2022),**
 316 **and the main Chhota Shigri (area-weighted) (Table 1) for a direct comparison with the**
 317 **traditional and nonlinear MBs that include the WT glacier.**

318 **3.6 Homogenization of glacier-wide mass balances**

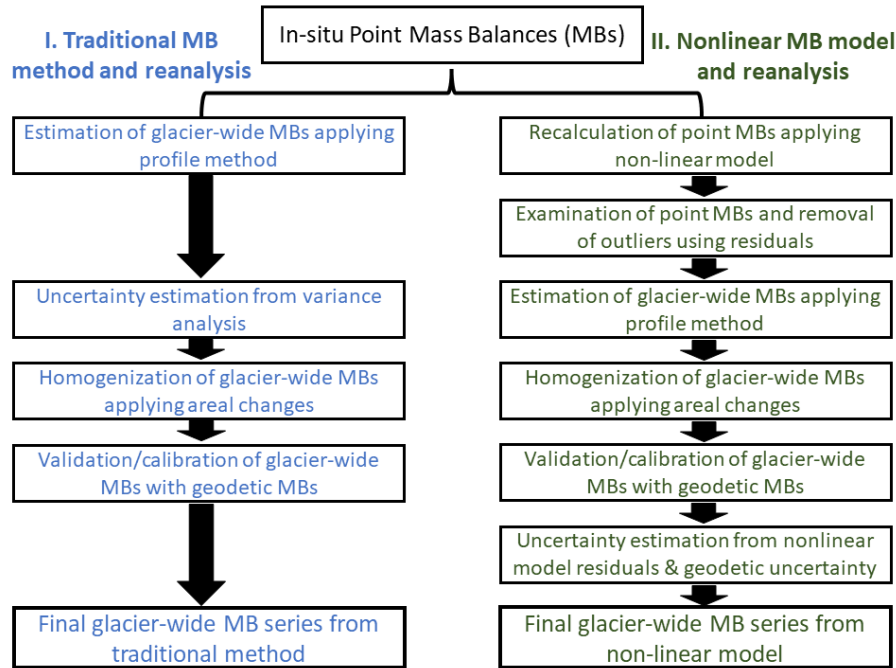
319 In initial studies (Wagnon et al., 2007; Azam et al., 2012), a fixed hypsometry (glacier area
 320 and elevation) from SPOT5 2005 DEM was used, while in follow-up studies (Azam et al.,
 321 2014; Mandal et al., 2020) a fixed hypsometry from Pléiades August 2014 DEM was used to
 322 estimate the traditional MBs on Chhota Shigri Glacier. These fixed hypsometries insert bias
 323 in the MB series (Cogley et al., 2011; Zemp et al., 2013). Here, the Chhota Shigri Glacier
 324 annual MBs (from the traditional method and nonlinear model) are homogenized with the
 325 linearly changing annual hypsometries from ASTER and Pléiades DEMs over 2003–2014
 326 and Pléiades DEMs over 2014–2020 (section 4.1). We adopted the approach suggested by
 327 Zemp et al. (2013) that assumes a linear area change over a record period (N years) and
 328 estimates the area (s) of an elevation band (e) for each year (t) as follows:

329

$$330 \quad s_{e,t} = s_{e,0} + \frac{t}{N} \cdot (s_{e,N} - s_{e,0}), \quad (3)$$

331

332 where $s_{e,0}$ and $s_{e,N}$ are the elevation bin areas from the first and the second geodetic survey,
 333 respectively, and the time t is zero in the year of the first survey. The homogenization process
 334 of both traditional and nonlinear MB series changed the annual glacier-wide MBs at most by
 335 0.02 m w.e., reflecting the negligible impact of areal changes over the 2003–2020 period on
 336 Chhota Shigri Glacier (section 4.1). Post-2020, the hypsometry of the 2020 year was used to
 337 estimate the MBs till 2023. Figure 5 summarizes the overall methodology step-by-step,
 338 including homogenization, validation/calibration and error estimation (sections 3.7 and 3.9).



339

340 **Figure 5:** Conceptual diagram of the overall methodology: homogenization, uncertainty
 341 estimation, validation, and calibration steps.

342 3.7 Validation and calibration of glacier-wide mass balances

343 Previously, we validated the traditional MBs with geodetic MB available over 2005–2014
 344 (Azam et al., 2016). The systematic biases were within the uncertainty ranges of traditional
 345 and geodetic MBs; hence, no calibration was done. In this study, we repeated this validation
 346 over two periods **for which** the geodetic MBs were calculated (section 4.2).

347 The traditional as well as nonlinear MBs over 2003–2014 were not statistically
 348 different from the geodetic MB, and the null hypothesis H_0 (the cumulative glaciological MB
 349 is not statistically different from the geodetic MB) was accepted at 95% and 90% levels
 350 (Zemp et al., 2013). However, over 2014–2020, both traditional and nonlinear MBs were
 351 statistically different from the geodetic MBs, and the null hypothesis H_0 was rejected at 95%
 352 as well as 90% levels. This showed that the systematic biases were significant over

353 2014–2020 (Table 2). Even though we did not observe a significant bias over 2003–2014, we
 354 decided to calibrate the traditional as well as nonlinear MBs over both periods as suggested in
 355 previous studies (Thibert et al., 2008; Huss et al., 2009; Andreassen et al., 2016; Wagnon et
 356 al., 2021).

357 In the calibration procedure, the annual relative variability of glacier-wide MBs is
 358 taken from the MB series and the series was fitted to the multi-annual geodetic MB, B_g , as
 359 follows:

$$360 \quad B_{a,cal} = B_a + \frac{(B_g - \sum_N B_a)}{N}, \quad (4)$$

361 where $B_{a,cal}$ is the annual calibrated glacier-wide MB and N is the number of years over
 362 which the geodetic MB has been estimated. It should be mentioned that the MBs obtained
 363 from traditional method or nonlinear model refer only to the surface MB, whereas the
 364 geodetic MBs also integrate the internal and basal MBs, assumed to be small compared to the
 365 surface MB (Cuffey and Paterson, 2010).

366 **3.8 Calibration of mean altitudinal mass balances**

367 The mean altitudinal MBs ($b_{e,t}$) for each 50-m elevation band (e) and each year (t) were
 368 computed using equation 1 exploiting the values of α_i , β_t and γ_i obtained from the nonlinear
 369 model. These altitudinal mean MBs were adjusted to fit the calibrated annual glacier-wide
 370 MBs following Zemp et al. (2013). **The calibrated altitudinal mean MB ($b_{e,t,cal}$) for each year**
 371 **is estimated as:**

$$372 \quad b_{e,t,cal} = b_{e,t} - B_a + B_{a,cal}, \quad (5)$$

373 **where B_a is the uncalibrated annual nonlinear MBs and $B_{a,cal}$ is the calibrated annual**
 374 **nonlinear MBs.** The equilibrium line altitude (ELA_{cal}) and MB gradient for each year (t) are
 375 also estimated by plotting the linear regression over the calibrated annual mean altitudinal
 376 MBs ($b_{e,t,cal}$) over an elevation range of 4375-5225 m. Finally, using the calibrated $ELAs$, the
 377 calibrated $AARs$ were estimated each year (Table 3).

378 **3.9 Random error estimation in nonlinear mass balances**

379 The random error ($\sigma_{B_{n,cal}}$) in calibrated nonlinear glacier-wide MB is estimated following:

$$380 \quad \sigma_{B_{n,cal}} = \pm \sqrt{\frac{\sigma_{B_g}^2}{N} + \sum s_i^2 \sigma_\varepsilon^2}, \quad (6)$$

381

382 σ_{B_g} is the error in the geodetic MBs ($\sigma_{B_g} = 0.57$ and 0.36 m w.e. a^{-1} over 2003–2014 and
383 2014–2020, respectively), N is the number of years for geodetic MB estimation (section 3.3),
384 s_i terms represent the relative areas of each 50-m elevation band (except for 5400–5850 m
385 a.s.l. range that has been treated as a single band) compared to the total glacier area (therefore
386 $\sum s_i = 1$), and $\sigma_\varepsilon = 0.30$ m w.e. a^{-1} is the standard deviation of the residual term of equation
387 (2) obtained with the nonlinear model (section 3.2). Equation 6 is valid for the hydrological
388 years within calibration periods (2003–2014 and 2014–2020). The random errors in nonlinear
389 glacier-wide MBs for 2002/03 and 2020–2023 hydrological years were estimated following
390 the procedure described in Wagnon et al. (2021). The mean annual random error, $\sigma_{B_{n,cal}}$, of
391 the calibrated nonlinear glacier-wide MB was estimated to be ± 0.19 m w.e. a^{-1} over 2002–
392 2023, with slightly higher random errors for the years outside the calibration period (Table 3).

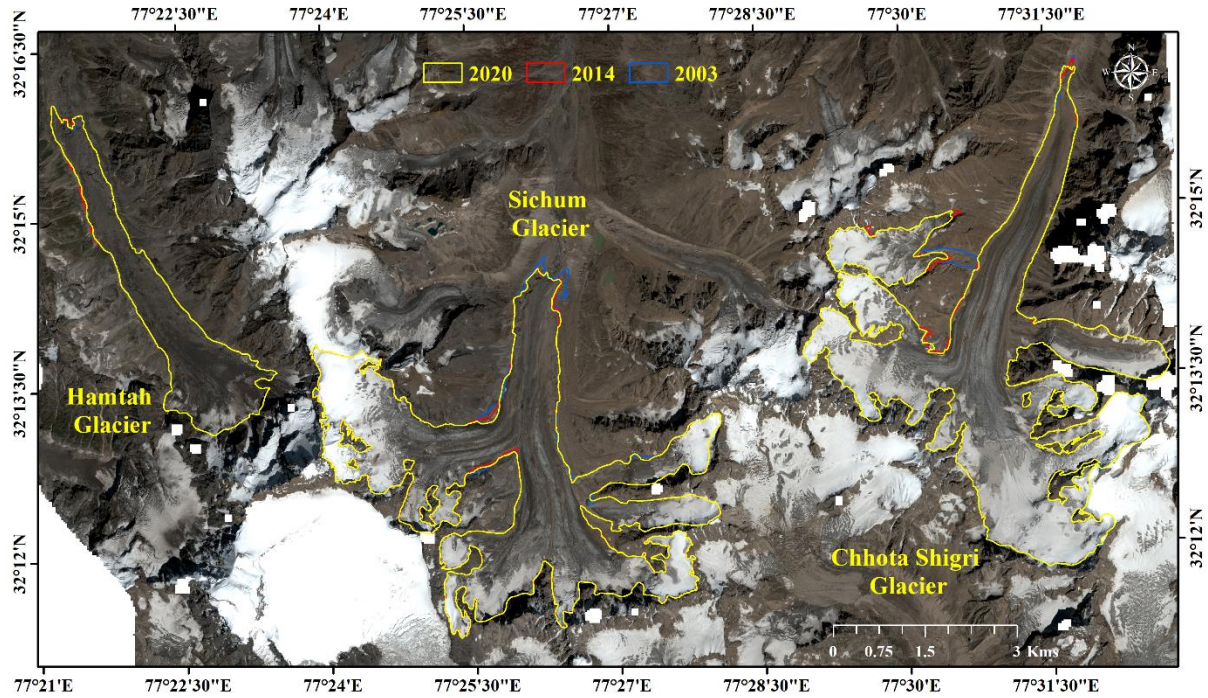
393 **4. Results**

394 **4.1 Glacier area changes since 2003**

395 Chhota Shigri, Sichum and Hamtah glaciers showed limited areal changes since 2003, mostly
396 restricted to the snout area (Table 1; Fig. 6). The estimated debris cover, corresponding to
397 September 2020 year, was 12%, 22% and 79% of the total area on Chhota Shigri, Sichum and
398 Hamtah glaciers, respectively (Table 1). During 2003–2020, the total area change for each
399 glacier was very small with a deglaciation rate of -0.07 ± 0.22 % a^{-1} , -0.07 ± 0.22 % a^{-1} and
400 -0.03 ± 0.19 % a^{-1} for Chhota, Sichum and Hamtah, respectively (Table 1).

401 **4.2 Geodetic mass balances**

402 The maps of elevation changes for 2003–2014 and 2014–2020 periods indicate a general
403 pattern of thinning for the glacier tongues and limited changes in the upper reaches of the
404 glaciers (Fig. 7). The area-weighted geodetic MB of Chhota Shigri Glacier (including WT)
405 was -0.43 ± 0.08 m w.e. a^{-1} over 2003–2020 (Table 1), with a higher annual wastage of -0.51
406 ± 0.06 m w.e. a^{-1} over 2014–2020 compared to -0.38 ± 0.10 m w.e. a^{-1} over 2003–2014
407 (Table 2). Sichum and Hamtah glaciers showed slightly stronger annual mass wastage of
408 -0.57 ± 0.08 and -0.51 ± 0.08 m w.e. a^{-1} , respectively over 2003–2020, with similarly an
409 increased mass wastage over the recent period (2014–2020) (Table 1). The slightly more
410 negative glacier-wide MBs on all these glaciers during 2014–2020 agree with a recent study
411 suggesting an increased wastage over the recent decade in the Himalaya (Hugonnet et al.,
412 2021).



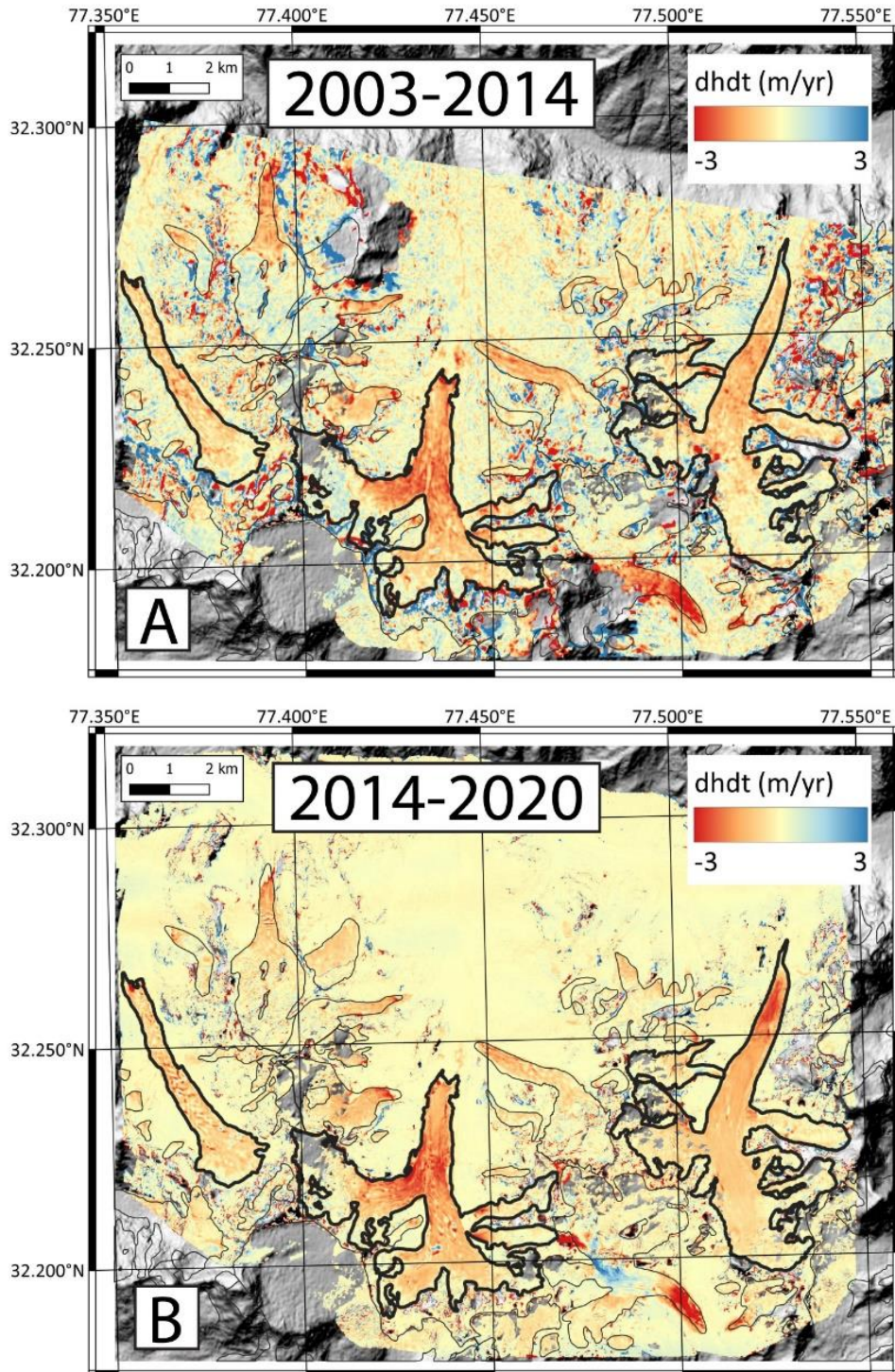
413

414 **Figure 6:** Glacier area change of Chhota Shigri, Sichum and Hamtah glaciers between 2003
 415 and 2020 (Background image is Pleiades satellite imagery of 12 September 2020; CNES
 416 2020, Distribution Airbus D&S).

417

418 **Table 1:** The areal and geodetic mass changes on Chhota Shigri, Sichum and Hamtah
 419 glaciers over the 2003-2014 and 2014-2020 periods.

Time Period	2003-14	2014-2020	2003-2020
Chhota Shigri with WT (Area = 15.47 km², 12% debris cover in 2020)			
Area change (km ²)	-0.15 ± 0.58	-0.05 ± 0.14	-0.20 ± 0.57
Area change rate (% a ⁻¹)	-0.09 ± 0.33	-0.05 ± 0.15	-0.07 ± 0.22
Geodetic MB (m w.e.)	-4.18 ± 0.57	-3.08 ± 0.36	-7.26 ± 0.93
Geodetic MB (m w.e. a ⁻¹)	-0.38 ± 0.10	-0.51 ± 0.06	-0.43 ± 0.08
Sichum (Area = 13.84 km², 22% debris cover in 2020)			
Area change (km ²)	-0.14 ± 0.52	-0.02 ± 0.12	-0.16 ± 0.52
Area change rate (% a ⁻¹)	-0.09 ± 0.34	-0.03 ± 0.14	-0.07 ± 0.22
Geodetic MB (m w.e.)	-6.07 ± 0.66	-3.68 ± 0.36	-9.75 ± 1.02
Geodetic MB (m w.e. a ⁻¹)	-0.55 ± 0.09	-0.61 ± 0.06	-0.57 ± 0.08
Hamtah (Area = 4.12 km², 79% debris cover in 2020)			
Area change (km ²)	-0.02 ± 0.13	-0.00 ± 0.03	-0.02 ± 0.13
Area change rate (% a ⁻¹)	-0.05 ± 0.29	-0.01 ± 0.13	-0.03 ± 0.19
Geodetic MB (m w.e.)	-5.19 ± 0.55	-3.44 ± 0.36	-8.63 ± 0.91
Geodetic MB (m w.e. a ⁻¹)	-0.47 ± 0.09	-0.57 ± 0.06	-0.51 ± 0.08



420

421 **Figure 7:** The thickness changes for Chhota Shigri, Sichum and Hamtah glaciers differencing
 422 the ASTER 2003 (08/10/2003) and Pléiades (26/09/2014) DEMs over 2003–2014 and
 423 Pléiades DEMs (26/09/2014 and 12/09/2020) over 2014–2020.

424 The mean annual geodetic mass wastage of -0.43 ± 0.08 m w.e. a^{-1} on Chhota Shigri
 425 Glacier over 2003–2020 is in good agreement with the region-wide mean glacier mass

426 wastage of -0.37 ± 0.15 m w.e. a^{-1} over the whole Lahaul-Spiti region (glacierized area =
 427 7960 km²) during a slightly different period (2000–2016), from multiple ASTER DEMs
 428 (Brun et al., 2017). Hence, Chhota Shigri is a reference glacier in the Himalaya (Azam, 2021)
 429 and a representative glacier for the whole Lahaul-Spiti region, as already suggested (Vincent
 430 et al., 2013).

431 4.3 Annual and cumulative glacier-wide mass balances since 2002

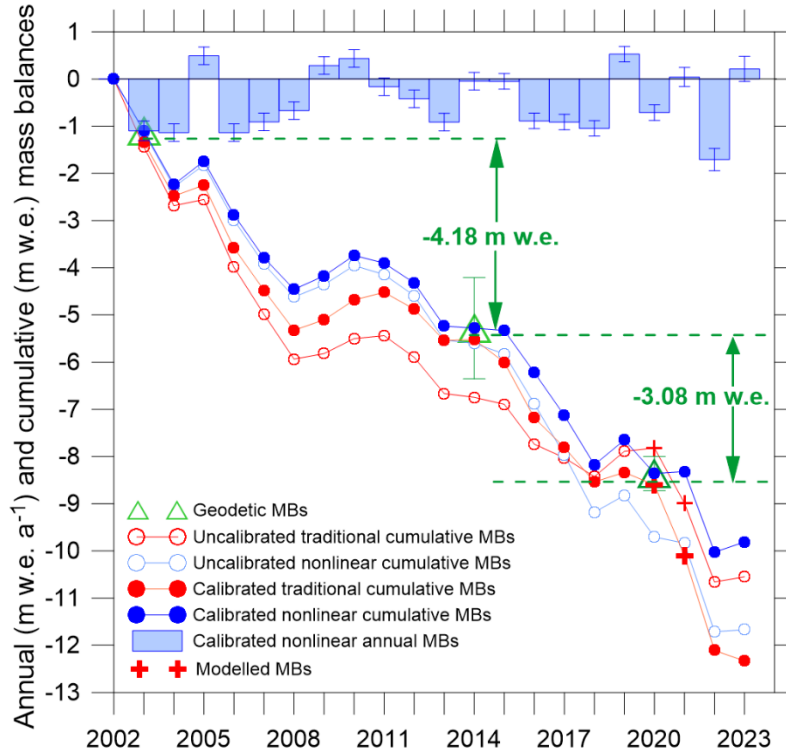
432 Table 2 and Fig. 8 show the traditional and nonlinear MBs (before and after calibration) and
 433 geodetic MBs over available periods. The traditional MBs were not available for 2019/20 and
 434 2020/21 (section 3.1); therefore, to calibrate these MBs and to cover the geodetic
 435 observations, the modelled MBs (2019/20 = 0.07 m w.e. and 2020/21 = -1.17 m w.e.) from
 436 surface energy balance approach (Srivastava and Azam, 2022b) were added to the series.

437 Compared to uncalibrated traditional MB series, uncalibrated nonlinear MB series
 438 showed much lesser biases with a slightly negative bias of -0.03 m w.e. a^{-1} (against a bias of
 439 -0.10 m w.e. a^{-1} in traditional MBs) over 2003–2014 and of -0.17 m w.e. a^{-1} (against a bias
 440 of 0.33 m w.e. a^{-1} in traditional MBs) over 2014–2020 (Table 2; Fig. 8). Therefore, following
 441 equation 4, the nonlinear annual MBs were systematically increased by 0.03 m w.e. a^{-1} over
 442 2003–2014 and by 0.17 m w.e. a^{-1} over 2014–2020 while traditional MBs were
 443 systematically increased by 0.10 m w.e. a^{-1} over 2003–2014 and decreased by 0.33 m w.e. a^{-1}
 444 over 2014–2020 to match the geodetic estimates (Fig. 8). The hydrological years 2002/03 and
 445 2020–2023 are outside the calibration periods, but these years were also calibrated by the
 446 mean values of biases observed over 2003–2014 and 2014–2020, respectively. To avoid
 447 confusion, we discussed only the calibrated nonlinear glacier-wide MBs in the manuscript,
 448 although the calibrated traditional MBs are given in Tables 2 and 3 for reference.

449 **Table 2:** Cumulative MBs (in parenthesis, mean annual MBs) from the traditional method,
 450 nonlinear model, and geodetic estimates over available periods. The balance year 2002/03 is
 451 not included here as it is not covered in the geodetic estimate available over 2003–2014. The
 452 cumulative traditional MB over the 2014–2020 period has been estimated by adding the
 453 modelled annual MB for 2019/20 (Srivastava and Azam, 2022b). All units are in m w.e. (m
 454 w.e. a^{-1}).

	2003–2014	2014–2019	2014–2020
Traditional MB	-5.31 (-0.48)	-1.14 (-0.23)	-1.07 (-0.18)*
Nonlinear MB	-4.48 (-0.41)	-3.22 (-0.64)	-4.10 (-0.68)
Geodetic MB	-4.18 (-0.38)	-	-3.08 (-0.51)
Calibrated traditional MB	-4.18 (-0.38)	-2.82 (-0.56)	-3.08 (-0.51)
Calibrated nonlinear MB	-4.18 (-0.38)	-2.37 (-0.47)	-3.08 (-0.51)

455 *estimated from traditional MBs (2014-2019) and modelled MB (2019/20).



456

457 **Figure 8:** Calibrated nonlinear annual glacier-wide MBs (with random errors) over
 458 2002–2023, traditional cumulative MBs over 2002–2023, nonlinear cumulative MBs over
 459 2002–2023, calibrated nonlinear cumulative MBs over 2002–2023, calibrated traditional
 460 cumulative MBs over 2002–2023, and geodetic MBs over 2003–2014 and 2014–2020 (with
 461 estimated uncertainties). The cumulative traditional MB series (2002–2019) is completed till
 462 2023 by adding the modelled MB of 2019/2020 and 2020/21 from Srivastava and Azam
 463 (2022b).

464 **Table 3:** Calibrated nonlinear MBs ($B_{a_n,cal}$), calibrated traditional MBs ($B_{a_t,cal}$), MB gradients
 465 (db/dz), ELA_{cal} and AAR_{cal} on Chhota Shigri Glacier between 2002 and 2023.

Year	Glacier Area (km ²)	$B_{a_n,cal}$ (m w.e. a ⁻¹)	Error of $B_{a_n,cal}$ (m w.e. a ⁻¹)	$B_{a_t,cal}$ (m w.e. a ⁻¹)	db/dz (m w.e. (100) ⁻¹ a ⁻¹)	ELA_{cal} (m a.s.l.)	AAR_{cal} (%)	Difference $B_{a_n,cal} - B_{a_t,cal}$
2002/03	15.66	-1.10	0.21	-1.34	0.70	5145	33	0.24
2003/04	15.64	-1.14	0.19	-1.14	0.71	5156	32	0.01
2004/05	15.63	0.49	0.19	0.24	0.59	4911	67	0.26
2005/06	15.61	-1.14	0.19	-1.33	0.71	5157	32	0.19
2006/07	15.59	-0.91	0.19	-0.90	0.69	5128	36	-0.01
2007/08	15.57	-0.67	0.19	-0.84	0.67	5096	40	0.17
2008/09	15.56	0.29	0.19	0.22	0.60	4942	63	0.07
2009/10	15.54	0.43	0.19	0.42	0.59	4921	65	0.01
2010/11	15.52	-0.16	0.19	0.17	0.64	5022	50	-0.33
2011/12	15.50	-0.42	0.19	-0.36	0.66	5061	44	-0.06
2012/13	15.49	-0.91	0.19	-0.66	0.69	5131	34	-0.25
2013/14	15.47	-0.05	0.19	0.02	0.63	5004	53	-0.07
2014/15	15.46	-0.05	0.16	-0.48	0.64	5027	50	0.43
2015/16	15.45	-0.89	0.16	-1.18	0.70	5148	33	0.29
2016/17	15.44	-0.91	0.16	-0.62	0.70	5151	31	-0.29
2017/18	15.44	-1.05	0.16	-0.73	0.71	5167	30	-0.32
2018/19	15.43	0.53	0.16	0.21	0.60	4930	64	0.32
2019/20	15.42	-0.71	0.16	-0.26	0.69	5125	35	-0.45
2020/21	15.42	0.04	0.20	-1.49	0.63	5013	51	1.53
2021/22	15.42	-1.71	0.24	-2.00	0.76	5248	19	0.29
2022/23	15.42	0.21	0.27	-0.22	0.62	4985	56	0.44
Mean	15.51	-0.47	0.19	-0.58	0.66	5070	44	0.12
SD	0.08	0.65	0.02	0.67	0.05	97	14	0.42

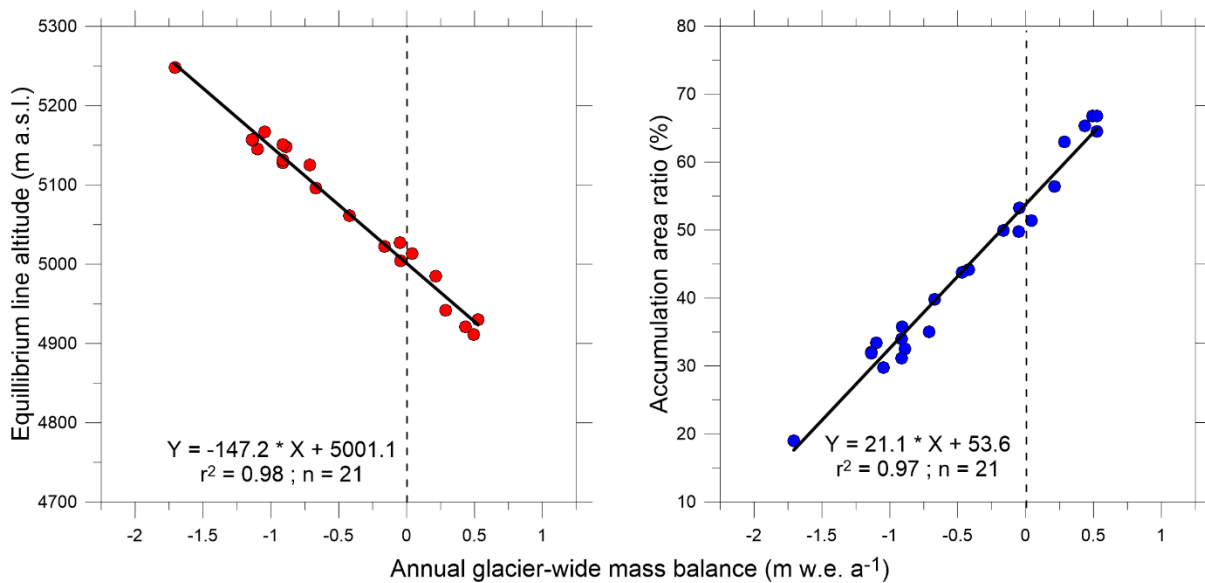
466 *The calibrated traditional MBs for 2019/20 and 2020/21 years are originally from the model (Srivastava and Azam, 2022b).

467 The annual calibrated glacier-wide MB from the nonlinear model varied from $0.53 \pm$
 468 $0.16 \text{ m w.e. a}^{-1}$ in 2018/19 to $-1.71 \pm 0.24 \text{ m w.e. a}^{-1}$ in 2021/22 with a standard deviation of
 469 $0.65 \text{ m w.e. a}^{-1}$ during 2002–2023 (Table 3). In the 21-year-long MB series, six hydrological
 470 years (2004/05, 2008/09, 2009/10, 2018/19, 2020/21, and 2022/23 showed positive/near
 471 steady state MBs. The mean annual glacier-wide MB was estimated to be $-0.47 \pm 0.19 \text{ m}$
 472 w.e. a^{-1} , equivalent to a cumulative loss of $-9.81 \pm 0.87 \text{ m w.e.}$ over 2002–2023 (Table 3).
 473 **The uncertainty in cumulative mass loss comes from error propagation law.**

474 4.4 Equilibrium line altitude and accumulation area ratio

475 Using the calibrated mean altitudinal MBs (section 3.8), the equilibrium line altitude ELA_{cal} ,
 476 accumulation area ratio AAR_{cal} and MB gradients (db/dz) were also estimated. The maximum
 477 ELA_{cal} was 5248 m a.s.l. corresponding to the most negative MB of $-1.71 \pm 0.24 \text{ m w.e. a}^{-1}$
 478 and minimum AAR_{cal} of 19% in 2021/22, while the minimum ELA_{cal} was 4911 m a.s.l.
 479 corresponding to a positive MB of $0.49 \pm 0.19 \text{ m w.e. a}^{-1}$ and a maximum AAR_{cal} of 67% in
 480 2004/05. The mean ELA_{cal} was 5070 m a.s.l. corresponding to a mean mass wastage of -0.47
 481 $\pm 0.19 \text{ m w.e. a}^{-1}$ and mean AAR_{cal} of 44% over 2002-2023.

482 The annual ELA_{cal} and AAR_{cal} showed good correlations with annual glacier-wide
 483 MBs ($r^2 = 0.98$ and 0.97 , respectively) over 2002-2023 (Fig. 5). The ELA_{cal} for a zero
 484 glacier-wide MB (ELA_0) was also computed from the regression between glacier-wide MBs
 485 and ELA_{cal} over 2002-2023 and calculated as $\sim 5001 \text{ m a.s.l.}$ (Fig. 9). Similarly, AAR_0 was
 486 computed as $\sim 54\%$ for steady-state glacier-wide MB.

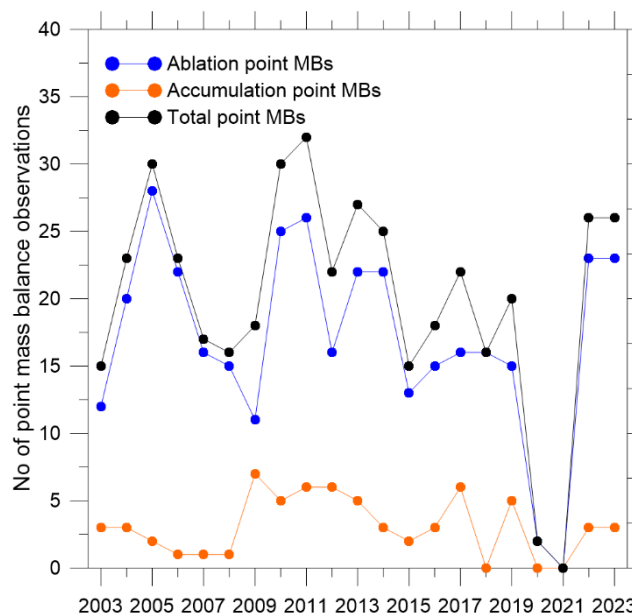


487
 488 **Figure 9:** The ELA and AAR as a function of annual glacier-wide MB.
 489

490 5. Discussion

491 5.1 Biases in glacier-wide mass balances and performance of nonlinear model

492 A total of 358 annual ablation and 65 annual accumulation point measurements were
493 collected on Chhota Shigri Glacier over 2002–2023 to estimate the glacier-wide MBs (five
494 ablation and five accumulation point MB measurements were removed before final model
495 run; section 3.3). Figure 10 shows the temporal evolution of the number of these point
496 measurements, and Table S1 provides the details about these point MBs. In general, the point
497 MB measurement network (especially the accumulation points) has been poor after 2014
498 (section 3.1, Fig. 10). The eastern accumulation site at 5550 m a.s.l. (Fig. 1) could only be
499 accessed five times (2003, 2004, 2005, 2009, 2011) over the 2002–2023 period, while no
500 accumulation measurements were done in 2018, 2020 and 2021 (section 3.1). Occasionally,
501 the ablation measurements were also missing due to missing stakes (heavy ablation or
502 destroyed stakes). In the traditional method, these missing measurements were filled with
503 extrapolated values from nearby ablation/accumulation MB measurements or previous years’
504 point MB measurements to estimate the glacier-wide MBs (Azam et al., 2016; Mandal et al.,
505 2020; Table S1).



506

507 **Figure 10:** Number of available ablation, accumulation, and total point MBs for each
508 hydrological year between 2002 and 2023.

509 The systematic biases in glacier-wide annual MB series with the same monitoring
510 network are expected to be of the same sign throughout the observation period, and the series
511 is systematically adjusted to match the geodetic MBs available over one or more periods
512 (Zemp et al., 2013; Wagnon et al., 2021). Nonlinear MB series on Chhota Shigri Glacier

513 showed negative biases (-0.03 and -0.17 m w.e. a^{-1} over the 2003-2014 and 2014-2020
514 periods, respectively), suggesting that the nonlinear model can reasonably estimate the
515 glacier-wide MBs with the existing monitoring network. Conversely, the traditional MB
516 series showed a negative bias (-0.10 m w.e. a^{-1}) over the 2003-2014 period and a large,
517 positive bias (0.33 m w.e. a^{-1}) over the 2014-2020 (Fig. 8; Table 2). The major disagreement
518 between the cumulative nonlinear and traditional MB curves after 2017 (Fig. 8) is likely due
519 to a degradation of the quality of field observations due to harsh weather, too short field
520 surveys, or observers **not being sufficiently experienced** (Fig. 10; Table S1; section 3.1).
521 **Wagnon et al. (2021) performed a thorough analysis on Mera Glacier (Dush Koshi Basin,**
522 **Nepal) and identified the precise source of systematic bias in the glacier-wide MB by**
523 **comparing the surface-specific mass balance calculated using the traditional glaciological**
524 **method of a specific zone on the glacier with that derived from the ice-flux method (based on**
525 **the mass conservation equation). Unfortunately, we could not conduct such an analysis in the**
526 **current study due to insufficient data availability. However, future research will include this**
527 **comparative analysis to uncover any systematic biases in the glacier-wide MB data series for**
528 **the Chhota Shigri Glacier.**

529 To further investigate the performance of the nonlinear model compared to the
530 traditional MB method, we calibrated both the MB series with the geodetic MB estimated
531 using ASTER (08/10/2003) and Pléiades (12/09/2020) DEMs (details in SI) and used the
532 geodetic MB over 2003–2014 (section 4.2) to validate both the calibrated series. The
533 calibrated nonlinear MB series showed a good agreement with the available geodetic MB
534 (-3.88 m w.e. against -4.18 m w.e.), while the traditional MB showed very strong deviation
535 from the geodetic MB over 2003–2014 (-6.13 m w.e. against -4.18 m w.e.) (Fig. S1). This
536 good agreement between nonlinear and geodetic MBs over 2003-2014 shows the robustness
537 of the nonlinear model for the glacier-wide mass balance estimation. Further, this
538 comparison also highlights the importance of using short-duration geodetic MB estimates for
539 the calibration process, as with two calibration periods, the calibrated traditional MB is in
540 better agreement with the geodetic MB (Fig. S1).

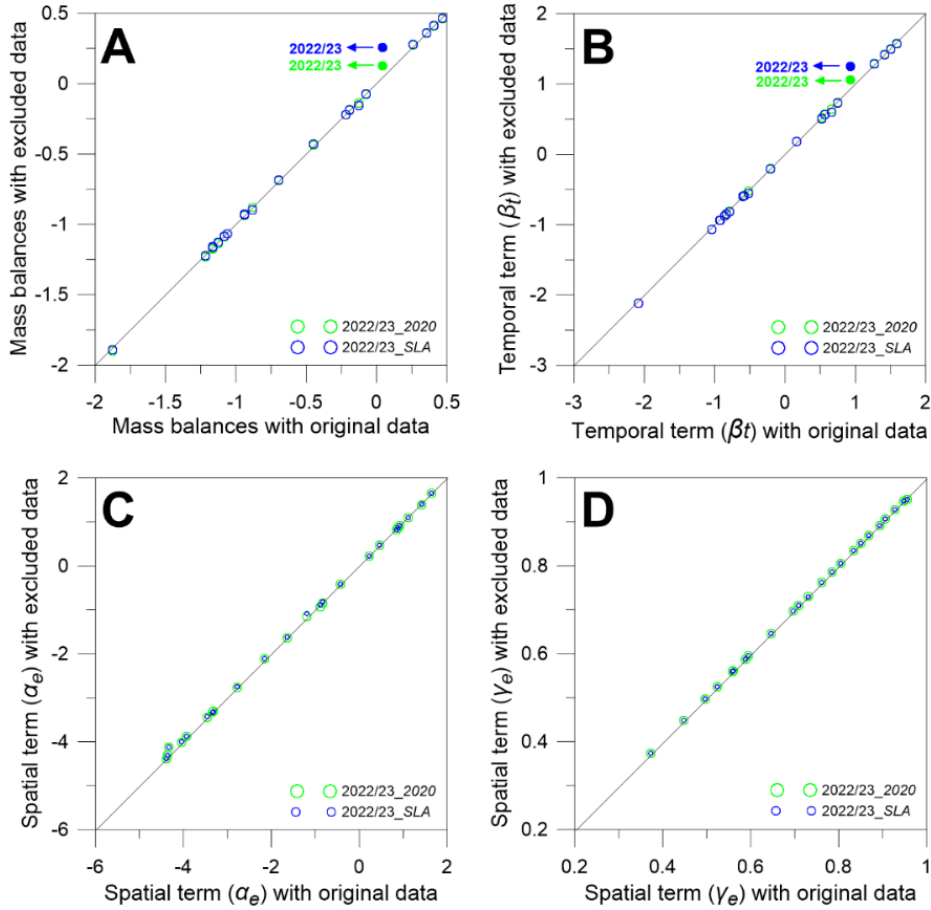
541 The nonlinear model shows a much better agreement with geodetic MBs than the
542 traditional method (Fig. 8; Table 2) mainly due to the (i) capability of the nonlinear model to
543 better capture the spatial variability of surface MB from a heterogeneous, discontinuous and
544 limited point MB data series than the traditional method (Vincent et al., 2018), (ii)
545 correction/exclusion of erroneous measurements (section 3.3) and (iii) exclusion of the
546 extrapolated ablation/accumulation points in the nonlinear model that might have introduced

547 biases in traditional MB (Fig. S2). The extrapolated point-MBs in the accumulation area
548 showed a difference ranging from -1.98 to 1.74 m w.e. between modelled and extrapolated,
549 especially post-2014 (Fig. S2 and S3). The better performance of the nonlinear model
550 suggests that the extrapolation of point accumulations (in case of missing point
551 measurements) in estimating the glacier-wide MB using the traditional method is risky.

552 **5.2 2019/20 glacier-wide mass balance from two point mass balances**

553 The spatial and temporal terms in equation (2) are computed from a data sample available
554 from the whole series; therefore, MB computation is expected to be affected by missing data
555 from any single year (or, in general, from all years whenever data is missing). The
556 glacier-wide MB for 2019/20 was estimated using only two point MB observations (section
557 3.2; Table S1); therefore, it might have biases (Lliboutry, 1974; Vincent et al., 2018).

558 To investigate the additional error, we selected the year 2022/23 to test the
559 performance of the nonlinear model. The 2022/23 year was selected because it is among the
560 years with the maximum of point MB observations, and they were performed at their original
561 locations. The nonlinear model was re-run over the 2002-2023 period, keeping only two point
562 MB data (out of 26) for 2022/23 year corresponding to the locations of the two point MB
563 measurements in 2019/20. With only two point MBs, the glacier-wide MB for 2022/23 was
564 recomputed to be 0.13 m w.e. a^{-1} against the original MB of 0.04 m w.e. a^{-1} with a difference
565 of 0.09 m w.e. a^{-1} , while all other year's glacier-wide MBs were changed by a maximum of
566 ± 0.01 m w.e. a^{-1} (Fig. 11A). As expected, the changes in the temporal term, β_t , having a
567 glacier-wide significance, showed significant deviation from 0.93 to 1.06 m w.e. a^{-1} for
568 2022/23 year, while for other years it changed by maximum up to ± 0.04 m w.e. a^{-1} (Fig.
569 11B). Conversely, the deviations in mean altitudinal spatial terms α_e and γ_e were very small
570 (maximum up to ± 0.06 m w.e. and ± 0.005 , respectively) (Fig. 11C, 11D). Therefore, the
571 temporal term (β_t) in equation (2) mainly controls the annual glacier-wide MB.



572

573 **Figure 11:** Glacier-wide MBs (A), temporal (β_t) (B) and spatial terms (α_e , and γ_e) (C and D,
 574 **respectively**) obtained with the nonlinear model following two different scenarios as a
 575 function of their original values obtained with the full dataset. In the first scenario
 576 (2022/23_2020), we remove all the data from 2022/23 (24-point MBs) except two located at
 577 the observation points in 2019/20 (see section 5.2). In the second scenario (2022/23_SLA), we
 578 remove all the data from 2022/23 and keep only two point MB data (= 0 m w.e.) obtained
 579 along the SLA (see section 5.3). The filled dots highlight the test year of 2022/23.

580 The deviation of 0.09 m w.e. a⁻¹ in glacier-wide MB estimated with only two point
 581 MBs is less than the estimated random error of 0.27 m w.e. a⁻¹ in the 2022/23 glacier-wide
 582 MB in the original model run; therefore, it is assumed that the error in 2019/20 glacier-wide
 583 MB due to restricted number of MB measurements is also less than the estimated random
 584 error of 0.16 m w.e. a⁻¹ (Table 3). Unlike the traditional MB method, the nonlinear model can
 585 fill the gaps in glacier-wide MB where some point MB observations are missing and can
 586 provide a consistent series of temporal fluctuations.

587 5.3 2020/21 glacier-wide mass balance from nonlinear model-SLA method

588 The glacier-wide MB for 2020/21 year was estimated by inferring two point MB input from
 589 end-of-summer SLA, assuming it to be equivalent to ELA (i.e., MB = 0 m w.e.) (section 3.2;

590 Fig. 3). Due to only two point MB input data, the modelled glacier-wide MB for 2020/21
591 may also have additional errors.

592 To quantify this error, we repeated the same exercise as in section 5.2 for the year
593 2022/23, this time keeping again two point MB data of 2022/23, but at the two sites where
594 point MB data have been assessed to be zero in 2020/21. The resulting 2022/23 glacier-wide
595 MB is 0.26 m w.e. a⁻¹, 0.22 m w.e. a⁻¹ higher than the original value (Fig. 11A), mainly
596 explained by the β_t term (Fig. 11B). This difference is still lower than the estimated random
597 error of 0.27 m w.e. a⁻¹ in 2022/23 (Table 3). However, there are still possible biases in
598 glacier-wide MB of 2020/21 year as the SLA was delineated from a Sentinel image from 6
599 September 2021 (section 3.2; Fig. 3) that is not exactly from the end of ablation season (30
600 September) on Chhota Shigri Glacier. The surface energy balance model estimated a MB of
601 -0.19 m w.e. over the 6 September – 30 September 2021 (Srivastava and Azam, 2022a).
602 However, this seasonal offset correction in SLA-derived annual MB may be given, but it was
603 avoided as the differences are within the estimated random error of 0.20 m w.e. a⁻¹ (Table 3).
604 Our analysis shows that the glacier-wide MB can also be estimated from SLA using the
605 nonlinear model if the field measurements cannot be carried out for some specific years.

606 However, the nonlinear model-SLA method has several limitations: (i) the delineated
607 SLA must pass through grid/s having previous point MB observation/s (Fig. 3) as at least one
608 previous measurement is required to run the model, (ii) the delineated SLA must be from the
609 end of ablation season to consider it as ELA, (iii) SLA delineation has its challenges and
610 often it is difficult to find the cloud-free image for delineation at the end of ablation season
611 (Brun et al., 2015; Racoviteanu et al., 2019), and (iv) SLA is severely affected by recent
612 snowfall hence must be checked with in-situ precipitation data before using SLA in nonlinear
613 model. This latter point implies that the ELA can be inferred from the end-of-ablation-season
614 SLA, which is not always possible over glaciers, especially in monsoon-dominated regions
615 (Brun et al., 2015).

616 **5.4 Recommendation: apply the nonlinear model on other glaciers**

617 This study demonstrates that the nonlinear model outperforms the traditional method for
618 estimating glacier-wide MB (section 5.1). Apart from the present research, the nonlinear
619 model has been applied only to the Mera Glacier in the Himalaya (Wagnon et al., 2021) and
620 on Argentière, Saint Sorlin, Mer de Glace, and Gébroulaz (France, Alps), Zongo (Bolivia,
621 Andes), and Nigardsbreen (Norway, Scandinavia) glaciers (Vincent et al., 2018).

622 Equation (1) includes a spatial effect term (γ_i) that accounts for the standard
623 deviations in point MBs across elevation. This term typically requires around ten years of
624 point MB observations to be accurately estimated (Vincent et al., 2018). Therefore, applying
625 the nonlinear model wherever MB observations are available for around ten years is
626 advisable, especially in the Himalaya where data accessibility issues often lead to gaps in
627 observations (Azam et al., 2018). We recommend extending the application of the nonlinear
628 model to other Himalayan glaciers that have consistent MB observations spanning
629 approximately ten years, such as Kolahoi, Hoksar and Sutri Dhaka glaciers in the western
630 Himalaya, and Chorabari, Dokriani Bamak, Pokalde, Rikha Samba, Yala, West Changri Nup
631 glaciers in the central Himalaya, etc. However, the estimated glacier-wide MBs may contain
632 systematic biases due to the distribution of point measurements across the glacier. Therefore,
633 they should be verified and, if necessary, reanalyzed using geodetic estimates.

634 **Conclusions**

635 This work reanalyses glacier-wide MBs by combining the traditional reanalysis framework
636 (Zemp et al., 2013) and the nonlinear MB model (Vincent et al., 2018). Previously, the
637 annual glacier-wide MBs had been estimated on Chhota Shigri Glacier since 2002, when the
638 traditional glaciological method was applied using heterogeneous in-situ point MB
639 measurements. The heterogeneous measurement network does not always catch the large
640 spatiotemporal variability of point MBs; hence, the point MB-elevation relationship is
641 insufficient to investigate the changes in glacier-wide MBs. Therefore, we applied the
642 nonlinear model to compute the glacier-wide MBs of Chhota Shigri Glacier as it enables the
643 computation of the glacier-wide MB from a heterogeneous in-situ point MB network. The
644 nonlinear model was used to detect the measurement errors. Five of the 423-point
645 measurements were corrected from field notebooks, and ten were recognized as wrong
646 observations and discarded before running the final model.

647 ASTER and Pléiades DEMs were used to estimate the geodetic MBs over 2003–2014
648 and 2014–2020 and they have been used to reanalyse the nonlinear MBs. Nonlinear MBs
649 agreed well with the geodetic estimates available over 2003–2014 and 2014–2020, unlike
650 traditional MBs that showed large differences, especially over the 2014–2020 period. The
651 reanalysed nonlinear MBs showed a large annual variability ranging from 0.53 ± 0.16 m w.e.
652 a^{-1} in 2018/19 to -1.71 ± 0.24 m w.e. a^{-1} in 2021/22. The Chhota Shigri Glacier is
653 imbalanced with a mean mass wastage of -0.47 ± 0.19 m w.e. a^{-1} , equivalent to a cumulative
654 loss of -9.81 ± 0.87 m w.e. over 2002–2023.

655 With the 21-year-long MB observations, the Chhota Shigri Glacier MB series is the
656 longest in the Himalaya. This work has enabled the data set to be extended, optimised, and
657 corrected to provide the best possible mass balance series for this benchmark glacier. We
658 plan to monitor this glacier over a long period, with repeated satellite image acquisitions by
659 the Pléiades Glacier Observatory to regularly validate/calibrate the glacier-wide MB,
660 typically every five years.

661 Our detailed analysis suggests that the nonlinear model performs better in calculating
662 the glacier-wide MB than the traditional method as (i) the nonlinear MBs are in much better
663 agreement with the geodetic MB estimates, (ii) it can detect erroneous measurements, (iii) it
664 provides better glacier-wide MBs than those of the traditional method when the observational
665 network is very limited, and (iv) glacier-wide MB can be computed using SLA if the
666 ablation-end SLA passes through a grid cell that contains point MB observations from
667 previous years. Therefore, the application of the nonlinear model is suggested on all
668 monitored glaciers whenever data is sufficient. It becomes even more relevant in the
669 Himalaya, where data are sometimes missing due to access issues. However, the estimated
670 glacier-wide MBs may contain systematic bias (arises from the distribution of point
671 measurements over the glacier) and, therefore, should be checked and, if necessary,
672 reanalysed with geodetic estimates.

673 **Author contribution**

674 MFA, CV and PW conceptualised the study. MFA did the nonlinear model runs and analysed
675 the data with the help of CV and PW. SS estimated the areal changes, the snow line altitudes,
676 and MBs from the energy balance model. EB estimated the geodetic MBs. MFA wrote the
677 paper with inputs from all co-authors.

678 **Competing interests**

679 At least one of the (co-)authors is a member of the editorial board of The Cryosphere.

680 **Acknowledgements**

681 MFA acknowledges the research grants from ISRO under the RESPOND scheme
682 (ISRO/RES/4/690/21-22), SERB (CRG/2020/004877) and MoES
683 (MOES/PAMC/H&C/131/2019-PC-II). EB acknowledges support from the French Space
684 Agency (CNES). Pléiades stereo-imagery of September 2020 was obtained through the
685 Pléiades Glacier Observatory. The authors are grateful to DST-IFCPAR/CEFIPRA project
686 n°3900-W1 and the French Service d'Observation GLACIOCLIM sponsored by IRD, which

687 provided financial support to conduct field trips and equipment. Thanks to all scientists,
688 Adhikari Ji and porters involved in the previous research expeditions on Chhota Shigri
689 Glacier since 2002.

690 **Code/Data Availability**

691 Detailed model documentation, tutorial and model codes can be found on the website of the
692 GLACIOCLIM program (<https://glacioclim.osug.fr>). The data used in this study can be
693 requested from the corresponding author.

694

695 **References**

696 Andreassen, L. M., Elvehøy, H., Kjøllmoen, B., and Engeset, R. V.: Reanalysis of long-term
697 series of glaciological and geodetic mass balance for 10 Norwegian glaciers, *The Cryosphere*,
698 10, 535–552, <https://doi.org/10.5194/tc-10-535-2016>, 2016.

699 Andreassen, L. M., Nagy, T., Kjøllmoen, B., and Leigh, J. R.: An inventory of Norway's
700 glaciers and ice-marginal lakes from 2018–19 Sentinel-2 data, *Journal of Glaciology*, 68,
701 1085–1106, <https://doi.org/10.1017/jog.2022.20>, 2022.

702 Azam, M. F.: Need of integrated monitoring on reference glacier catchments for future water
703 security in Himalaya, *Water Security*, 14, 100098,
704 <https://doi.org/10.1016/j.wasec.2021.100098>, 2021.

705 Azam, M. F., Wagnon, P., Ramanathan, A., Vincent, C., Sharma, P., Arnaud, Y., Linda, A.,
706 Pottakkal, J. G., Chevallier, P., Singh, V. B., and Berthier, E.: From balance to imbalance: a
707 shift in the dynamic behaviour of Chhota Shigri glacier, western Himalaya, India, *Journal of*
708 *Glaciology*, 58, 315–324, <https://doi.org/10.3189/2012JoG11J123>, 2012.

709 Azam, M. F., Wagnon, P., Vincent, C., Ramanathan, A., Linda, A., and Singh, V. B.:
710 Reconstruction of the annual mass balance of Chhota Shigri glacier, Western Himalaya,
711 India, since 1969, *Annals of Glaciology*, 55, 69–80,
712 <https://doi.org/10.3189/2014AoG66A104>, 2014.

713 Azam, M. F., Ramanathan, A., Wagnon, P., Vincent, C., Linda, A., Berthier, E., Sharma, P.,
714 Mandal, A., Angchuk, T., Singh, V. B., and Pottakkal, J. G.: Meteorological conditions,
715 seasonal and annual mass balances of Chhota Shigri Glacier, western Himalaya, India,
716 *Annals of Glaciology*, 57, 328–338, <https://doi.org/10.3189/2016AoG71A570>, 2016.

717 Azam, M. F., Wagnon, P., Berthier, E., Vincent, C., Fujita, K., and Kargel, J. S.: Review of
718 the status and mass changes of Himalayan-Karakoram glaciers, *Journal of Glaciology*, 64,
719 61–74, <https://doi.org/10.1017/jog.2017.86>, 2018.

720 Azam, M. F., Kargel, J. S., Shea, J. M., Nepal, S., Haritashya, U. K., Srivastava, S.,
721 Maussion, F., Qazi, N., Chevallier, P., Dimri, A. P., Kulkarni, A. V., Cogley, J. G., and
722 Bahuguna, I.: Glaciohydrology of the Himalaya-Karakoram, *Science*, 373, eabf3668,
723 <https://doi.org/10.1126/science.abf3668>, 2021.

724 Banerjee, A. and Shankar, R.: On the response of Himalayan glaciers to climate change,
725 *Journal of Glaciology*, 59, 480–490, <https://doi.org/10.3189/2013JoG12J130>, 2013.

726 Barandun, M., Pohl, E., Naegeli, K., McNabb, R., Huss, M., Berthier, E., Saks, T., and
727 Hoelzle, M.: Hot Spots of Glacier Mass Balance Variability in Central Asia, *Geophysical*
728 *Research Letters*, 48, e2020GL092084, <https://doi.org/10.1029/2020GL092084>, 2021.

729 Basantes-Serrano, R., Rabatel, A., Francou, B., Vincent, C., Maisincho, L., Cáceres, B.,
730 Galarraga, R., and Alvarez, D.: Slight mass loss revealed by reanalyzing glacier mass-balance
731 observations on Glacier Antisana 15 α (inner tropics) during the 1995–2012 period, *Journal of*
732 *Glaciology*, 62, 124–136, <https://doi.org/10.1017/jog.2016.17>, 2016.

733 Berthier, E., Arnaud, Y., Kumar, R., Ahmad, S., Wagnon, P., and Chevallier, P.: Remote
734 sensing estimates of glacier mass balances in the Himachal Pradesh (Western Himalaya,
735 India), *Remote Sensing of Environment*, 108, 327–338,
736 <https://doi.org/10.1016/j.rse.2006.11.017>, 2007.

737 Berthier, E., Floricioiu, D., Gardner, A. S., Gourmelen, N., Jakob, L., Paul, F., Treichler, D.,
738 Wouters, B., Belart, J. M. C., Dehecq, A., Dussaillant, I., Hugonnet, R., Kaab, A. M.,
739 Krieger, L., Pálsson, F., and Zemp, M.: Measuring Glacier Mass Changes from Space - A
740 Review, *Reports on Progress in Physics*, 86, 036801, <https://doi.org/10.1088/1361-6633/acaf8e>, 2023.

742 Bolch, T., Yao, T., Kang, S., Buchroithner, M. F., Scherer, D., Maussion, F., Huintjes, E.,
743 and Schneider, C.: A glacier inventory for the western Nyainqentanglha Range and the Nam
744 Co Basin, Tibet, and glacier changes 1976–2009, *The Cryosphere*, 4, 419–433,
745 <https://doi.org/10.5194/tc-4-419-2010>, 2010.

746 Bolch, T., Shea, J. M., Liu, S., Azam, F. M., Gao, Y., Gruber, S., Immerzeel, W. W.,
747 Kulkarni, A., Li, H., Tahir, A. A., Zhang, G., and Zhang, Y.: Status and Change of the
748 Cryosphere in the Extended Hindu Kush Himalaya Region, in: The Hindu Kush Himalaya
749 Assessment: Mountains, Climate Change, Sustainability and People, edited by: Wester, P.,
750 Mishra, A., Mukherji, A., and Shrestha, A. B., Springer International Publishing, Cham, 209–
751 255, https://doi.org/10.1007/978-3-319-92288-1_7, 2019.

752 Brun, F., Berthier, E., Wagnon, P., Käab, A., and Treichler, D.: A spatially resolved estimate
753 of High Mountain Asia glacier mass balances from 2000 to 2016, *Nature Geosci*, 10, 668–
754 673, <https://doi.org/10.1038/ngeo2999>, 2017.

755 Brun, F., Dumont, M., Wagnon, P., Berthier, E., Azam, M. F., Shea, J. M., Sirguey, P.,
756 Rabatel, A., and Ramanathan, A.: Seasonal changes in surface albedo of Himalayan glaciers
757 from MODIS data and links with the annual mass balance, *The Cryosphere*, 9, 341–355,
758 <https://doi.org/10.5194/tc-9-341-2015>, 2015.

759 Chand, P. and Sharma, M. C.: Frontal changes in the Manimahesh and Tal Glaciers in the
760 Ravi basin, Himachal Pradesh, northwestern Himalaya (India), between 1971 and 2013,
761 *International Journal of Remote Sensing*, 36, 4095–4113,
762 <https://doi.org/10.1080/01431161.2015.1074300>, 2015.

763 Cogley, J., Hock, R., Rasmussen, L., Arendt, A., Bauder, A., Braithwaite, R., Jansson, P.,
764 Kaser, G., Möller, M., Nicholson, L., and Zemp, M.: Glossary of glacier mass balance and
765 related terms, <https://doi.org/10.5167/uzh-53475>, 2011.

766 Cogley, J. G.: Geodetic and direct mass-balance measurements: comparison and joint
767 analysis, *Annals of Glaciology*, 50, 96–100, <https://doi.org/10.3189/172756409787769744>,
768 2009.

769 Cuffey, K. M. and Paterson, W. S. B.: *The Physics of Glaciers*, Academic Press, 721 pp.,
770 2010.

771 Davaze, L., Rabatel, A., Dufour, A., Hugonnet, R., and Arnaud, Y.: Region-wide annual
772 glacier surface mass balance for the European Alps from 2000 to 2016, *Frontiers in Earth*
773 *Science*, 8, 149, <https://doi.org/10.3389/feart.2020.00149>, 2020.

774 Falaschi, D., Bhattacharya, A., Guillet, G., Huang, L., King, O., Mukherjee, K., Rastner, P.,
775 Yao, T., and Bolch, T.: Annual to seasonal glacier mass balance in High Mountain Asia

776 derived from Pléiades stereo images: examples from the Pamir and the Tibetan Plateau, *The*
777 *Cryosphere*, 17, 5435–5458, <https://doi.org/10.5194/tc-17-5435-2023>, 2023.

778 Funk, M., Morelli, R., and Stahel, W.: Mass balance of Griesgletscher 1961-1994: Different
779 methods of determination, *Massenbilanz des Griesgletschers 1961-1994: Verschiedene*
780 *Bestimmungsverfahren*, 33, 41–56, 1997.

781 Gantayat, P. and Ramsankaran, R.: Modelling evolution of a large, glacier-fed lake in the
782 Western Indian Himalaya, *Sci Rep*, 13, 1840, <https://doi.org/10.1038/s41598-023-28144-8>,
783 2023.

784 Gardner, A., Moholdt, G., Cogley, J., Wouters, B., Arendt, A., Wahr, J., Berthier, E., Hock,
785 R., Pfeffer, W., Kaser, G., Ligtenberg, S., Bolch, T., Sharp, M., Hagen, J., Van den Broeke,
786 M., and Paul, F.: A Reconciled Estimate of Glacier Contributions to Sea Level Rise: 2003 to
787 2009, *Science (New York, N.Y.)*, 340, 852–857, <https://doi.org/10.1126/science.1234532>,
788 2013.

789 Garg, P. K., Shukla, A., and Jasrotia, A. S.: Influence of topography on glacier changes in the
790 central Himalaya, India, *Global and Planetary Change*, 155, 196–212,
791 <https://doi.org/10.1016/j.gloplacha.2017.07.007>, 2017.

792 Haq, M. A., Azam, M.F., Vincent, C.: Efficiency of artificial neural networks for glacier ice-
793 thickness estimation: a case study in western Himalaya, India. *Journal of Glaciology* 67(264),
794 671–684, <https://doi.org/10.1017/jog.2021.19>, 2021.

795 Harrison, S., Kargel, J. S., Huggel, C., Reynolds, J., Shugar, D. H., Betts, R. A., Emmer, A.,
796 Glasser, N., Haritashya, U. K., Klimeš, J., Reinhardt, L., Schaub, Y., Wiltshire, A., Regmi,
797 D., and Vilímek, V.: Climate change and the global pattern of moraine-dammed glacial lake
798 outburst floods, *The Cryosphere*, 12, 1195–1209, <https://doi.org/10.5194/tc-12-1195-2018>,
799 2018.

800 Hugonnet, R., McNabb, R., Berthier, E., Menounos, B., Nuth, C., Girod, L., Farinotti, D.,
801 Huss, M., Dussaillant, I., Brun, F., and Käab, A.: Accelerated global glacier mass loss in the
802 early twenty-first century, *Nature*, 592, 726–731, [https://doi.org/10.1038/s41586-021-03436-](https://doi.org/10.1038/s41586-021-03436-z)
803 [z](https://doi.org/10.1038/s41586-021-03436-z), 2021.

804 Huss, M., Bauder, A., and Funk, M.: Homogenization of long-term mass-balance time series,
805 *Annals of Glaciology*, 50, 198–206, <https://doi.org/10.3189/172756409787769627>, 2009.

806 Jackson, M., Azam, M. F., Baral, P., Benestad, R., Brun, F., Muhammad, S., Pradhananga, S.,
807 Shrestha, F., Steiner, J. F., and Thapa, A.: Chapter 2: Consequences of climate change for the
808 cryosphere in the Hindu Kush Himalaya, <https://doi.org/10.53055/ICIMOD.1030>, 2023.

809 Kuhn, M.: Mass Budget Imbalances as Criterion for a Climatic Classification of Glaciers,
810 *Geografiska Annaler. Series A, Physical Geography*, 66, 229–238,
811 <https://doi.org/10.2307/520696>, 1984.

812 Kumar, A., Verma, A., Gokhale, A., Bhambri, R., Misra, A., Sundriyal, S., Dobhal, D., and
813 kishore, N.: Hydrometeorological assessments and suspended sediment delivery from a
814 central Himalayan glacier in the upper Ganga basin, *International Journal of Sediment
815 Research*, 33, <https://doi.org/10.1016/j.ijsrc.2018.03.004>, 2018.

816 Laha, S., Kumari, R., Singh, S., Mishra, A., Sharma, T., Banerjee, A., Nainwal, H. C., and
817 Shankar, R.: Evaluating the contribution of avalanching to the mass balance of Himalayan
818 glaciers, *Annals of Glaciology*, 58, 110–118, <https://doi.org/10.1017/aog.2017.27>, 2017.

819 Lliboutry, L.: Multivariate Statistical Analysis of Glacier Annual Balances, *Journal of
820 Glaciology*, 13, 371–392, <https://doi.org/10.3189/S0022143000023169>, 1974.

821 Mandal, A., Ramanathan, A., Azam, M. F., Angchuk, T., Soheb, M., Kumar, N., Pottakkal, J.
822 G., Vatsal, S., Mishra, S., and Singh, V. B.: Understanding the interrelationships among mass
823 balance, meteorology, discharge and surface velocity on Chhota Shigri Glacier over 2002–
824 2019 using in situ measurements, *Journal of Glaciology*, 66, 727–741,
825 <https://doi.org/10.1017/jog.2020.42>, 2020.

826 Mandal, A., Angchuk, T., Azam, M. F., Ramanathan, A., Wagnon, P., Soheb, M., and Singh,
827 C.: An 11-year record of wintertime snow-surface energy balance and sublimation at
828 4863 m a.s.l. on the Chhota Shigri Glacier moraine (western Himalaya, India), *The
829 Cryosphere*, 16, 3775–3799, <https://doi.org/10.5194/tc-16-3775-2022>, 2022.

830 Miles, E., McCarthy, M., Dehecq, A., Kneib, M., Fugger, S., and Pellicciotti, F.: Health and
831 sustainability of glaciers in High Mountain Asia, *Nat Commun*, 12, 2868,
832 <https://doi.org/10.1038/s41467-021-23073-4>, 2021.

833 Mukherjee, K., Bhattacharya, A., Pieczonka, T., Ghosh, S., and Bolch, T.: Glacier mass
834 budget and climate reanalysis data indicate a climatic shift around 2000 in Lahaul-Spiti,

835 western Himalaya, *Climatic Change*, 148, 219–233, <https://doi.org/10.1007/s10584-018->
836 [2185-3](https://doi.org/10.1007/s10584-018-2185-3), 2018.

837 Nepal, S., Steiner, J. F., Allen, S., Azam, M. F., Bhuchar, S., Biemans, H., Dhakal, M.,
838 Khanal, S., Li, D., Lutz, A., Pradhananga, S., Ritzema, R., Stoffel, M., and Stuart-Smith, R.:
839 Chapter 3: Consequences of cryospheric change for water resources and hazards in the Hindu
840 Kush Himalaya, <https://doi.org/10.53055/ICIMOD.1031>, 2023.

841 Oerlemans, J.: *Glaciers and Climate Change*, CRC Press, 168 pp., 2001.

842 Østrem, G. and Stanley, A.: *Glacier mass balance measurements: a manual for field and*
843 *office work*. 1969.

844 Østrem, G. and Brugman, M.: *Glacier mass-balance measurements: a manual for field and*
845 *office work*, 1991.

846 Oulkar, S. N., Thamban, M., Sharma, P., Pratap, B., Singh, A. T., Patel, L. K., Pramanik, A.
847 and Ravichandran, M.: Energy fluxes, mass balance, and climate sensitivity of the Sutri
848 Dhaka Glacier in the western Himalaya. *Front. Earth Sci.* 10:949735.
849 [doi:10.3389/feart.2022.949735](https://doi.org/10.3389/feart.2022.949735) , 2022.

850 Rabatel, A., Dedieu, J.-P., and Vincent, C.: Using remote-sensing data to determine
851 equilibrium-line altitude and mass-balance time series: validation on three French glaciers,
852 1994–2002, *Journal of Glaciology*, 51, 539–546,
853 <https://doi.org/10.3189/172756505781829106>, 2005.

854 Racoviteanu, A. E., Rittger, K., and Armstrong, R.: An automated approach for estimating
855 snowline altitudes in the Karakoram and eastern Himalaya from remote sensing, *Frontiers in*
856 *Earth Science*, 7, 220, <https://doi.org/10.3389/feart.2019.00220>, 2019.

857 Ramsankaran, R., Pandit, A., and Azam, M. F.: Spatially distributed ice-thickness modelling
858 for Chhota Shigri Glacier in western Himalayas, India, *International Journal of Remote*
859 *Sensing*, 39, 3320–3343, <https://doi.org/10.1080/01431161.2018.1441563>, 2018.

860 Raup, B., Racoviteanu, A., Khalsa, S. J. S., Helm, C., Armstrong, R., and Arnaud, Y.: The
861 GLIMS geospatial glacier database: A new tool for studying glacier change, *Global and*
862 *Planetary Change*, 56, 101–110, <https://doi.org/10.1016/j.gloplacha.2006.07.018>, 2007.

863 Romshoo, S. A., Murtaza, K. O. & Abdullah, T.: Towards understanding various influences
864 on mass balance of the Hoksar Glacier in the Upper Indus Basin using observations. *Sci*
865 *Rep* **12**, 15669. <https://doi.org/10.1038/s41598-022-20033-w>, 2022.

866 Romshoo, S. A., Abdullah, T., Murtaza, K. O., Bhat, M. H.: Direct, geodetic and simulated
867 mass balance studies of the Kolahoi Glacier in the Kashmir Himalaya. India, *Journal of*
868 *Hydrology*, 617:129019. <https://doi.org/10.1016/j.jhydrol.2022.129019>, 2023.

869 Rounce, D. R., Hock, R., Maussion, F., Hugonnet, R., Kochtitzky, W., Huss, M., Berthier, E.,
870 Brinkerhoff, D., Compagno, L., Copland, L., Farinotti, D., Menounos, B., and McNabb, R.
871 W.: Global glacier change in the 21st century: Every increase in temperature matters,
872 *Science*, 379, 78–83, <https://doi.org/10.1126/science.abo1324>, 2023.

873 Shean, D. E., Bhushan, S., Montesano, P., Rounce, D. R., Arendt, A., and Osmanoglu, B.: A
874 Systematic, Regional Assessment of High Mountain Asia Glacier Mass Balance, *Frontiers in*
875 *Earth Science*, 7, <https://doi.org/10.3389/feart.2019.00363>, 2020.

876 Shugar, D. H., Jacquemart, M., Shean, D., Bhushan, S., Upadhyay, K., Sattar, A.,
877 Schwanghart, W., McBride, S., De Vries, M. V. W., Mergili, M., Emmer, A., Deschamps-
878 Berger, C., McDonnell, M., Bhambri, R., Allen, S., Berthier, E., Carrivick, J. L., Clague, J. J.,
879 Dokukin, M., Dunning, S. A., Frey, H., Gascoin, S., Haritashya, U. K., Huggel, C., Kääb, A.,
880 Kargel, J. S., Kavanaugh, J. L., Lacroix, P., Petley, D., Rupper, S., Azam, M. F., Cook, S. J.,
881 Dimri, A. P., Eriksson, M., Farinotti, D., Fiddes, J., Gnyawali, K. R., Harrison, S., Jha, M.,
882 Koppes, M., Kumar, A., Leinss, S., Majeed, U., Mal, S., Muhuri, A., Noetzli, J., Paul, F.,
883 Rashid, I., Sain, K., Steiner, J., Ugalde, F., Watson, C. S., and Westoby, M. J.: A massive
884 rock and ice avalanche caused the 2021 disaster at Chamoli, Indian Himalaya, *Science*, 373,
885 300–306, <https://doi.org/10.1126/science.abh4455>, 2021.

886 Shukla, A. and Qadir, J.: Differential response of glaciers with varying debris cover extent:
887 evidence from changing glacier parameters, *International Journal of Remote Sensing*, 37,
888 2453–2479, <https://doi.org/10.1080/01431161.2016.1176272>, 2016.

889 Shukla, A., Garg, P. K., and Srivastava, S.: Evolution of Glacial and High-Altitude Lakes in
890 the Sikkim, Eastern Himalaya Over the Past Four Decades (1975–2017), *Front. Environ. Sci.*,
891 6, 81, <https://doi.org/10.3389/fenvs.2018.00081>, 2018.

892 Soruco, A., Vincent, C., Francou, B., Ribstein, P., Berger, T., Sicart, J. E., Wagnon, P.,
893 Arnaud, Y., Favier, V., and Lejeune, Y.: Mass Balance of Glaciar Zongo, Bolivia, between

894 1956 and 2006, using glaciological, hydrological and geodetic methods, *Annals of*
895 *Glaciology*, 50, 1–8, <https://doi.org/10.3189/172756409787769799>, 2009.

896 Srivastava, S. and Azam, M. F.: Mass- and Energy-Balance Modeling and Sublimation
897 Losses on Dokriani Bamak and Chhota Shigri Glaciers in Himalaya Since 1979, *Frontiers in*
898 *Water*, 4, 874240, <https://doi.org/10.3389/frwa.2022.874240>, 2022a.

899 Srivastava, S. and Azam, Mohd. F.: Functioning of glacierized catchments in Monsoon and
900 Alpine regimes of Himalaya, *Journal of Hydrology*, 609, 127671,
901 <https://doi.org/10.1016/j.jhydrol.2022.127671>, 2022b.

902 Srivastava, S., Garg, P. K., and Azam, Mohd. F.: Seven Decades of Dimensional and Mass
903 Balance Changes on Dokriani Bamak and Chhota Shigri Glaciers, Indian Himalaya, Using
904 Satellite Data and Modelling, *J Indian Soc Remote Sens*, 50, 37–54,
905 <https://doi.org/10.1007/s12524-021-01455-x>, 2022.

906 Stokes, C. R., Clark, C. D., Lian, O. B., and Tulaczyk, S.: Ice stream sticky spots: A review
907 of their identification and influence beneath contemporary and palaeo-ice streams, *Earth-*
908 *Science Reviews*, 81, 217–249, <https://doi.org/10.1016/j.earscirev.2007.01.002>, 2007.

909 Stumm, D., Joshi, S. P., Gurung, T. R., and Silwal, G.: Mass balances of Yala and Rikha
910 Samba glaciers, Nepal, from 2000 to 2017. *Earth System Science Data*, 13(8), 3791–3818.
911 [doi:10.5194/essd-13-3791-2021](https://doi.org/10.5194/essd-13-3791-2021), 2021.

912 Sunako, S., Fujita, K., Sakai, A., and Kayastha, R.: Mass balance of Trambau Glacier,
913 Rolwaling region, Nepal Himalaya: In-situ observations, long-term reconstruction and mass-
914 balance sensitivity, *Journal of Glaciology* 65, 605–616. [doi:10.1017/jog.2019.37](https://doi.org/10.1017/jog.2019.37), 2019.

915 Tshering, P. and Fujita, K.: First in situ record of decadal glacier mass balance (2003–2014)
916 from the Bhutan Himalaya. *Annals of Glaciology*, 57(71), 289–294,
917 [doi:10.3189/2016AoG71A036](https://doi.org/10.3189/2016AoG71A036), 2016.

918 Thibert, E., Blanc, R., Vincent, C., and Eckert, N.: Glaciological and volumetric mass-
919 balance measurements: error analysis over 51 years for Glacier de Sarennes, French Alps,
920 *Journal of Glaciology*, 54, 522–532, <https://doi.org/10.3189/002214308785837093>, 2008.

921 Vincent, C., Ramanathan, A., Wagnon, P., Dobhal, D. P., Linda, A., Berthier, E., Sharma, P.,
922 Arnaud, Y., Azam, M. F., Jose, P. G., and Gardelle, J.: Balanced conditions or slight mass
923 gain of glaciers in the Lahaul and Spiti region (northern India, Himalaya) during the nineties

924 preceded recent mass loss, *The Cryosphere*, 7, 569–582, <https://doi.org/10.5194/tc-7-569->
925 [2013](https://doi.org/10.5194/tc-7-569-2013), 2013.

926 Vincent, C., Soruco, A., Azam, M. F., Basantes-Serrano, R., Jackson, M., Kjølmoen, B.,
927 Thibert, E., Wagnon, P., Six, D., Rabatel, A., Ramanathan, A., Berthier, E., Cusicanqui, D.,
928 Vincent, P., and Mandal, A.: A Nonlinear Statistical Model for Extracting a Climatic Signal
929 From Glacier Mass Balance Measurements, *Journal of Geophysical Research: Earth Surface*,
930 123, 2228–2242, <https://doi.org/10.1029/2018JF004702>, 2018.

931 Vishwakarma, B. D., Ramsankaran, R., Azam, M. F., Bolch, T., Mandal, A., Srivastava, S.,
932 Kumar, P., Sahu, R., Navinkumar, P. J., Tanniru, S. R., Javed, A., Soheb, M., Dimri, A. P.,
933 Yadav, M., Devaraju, B., Chinnasamy, P., Reddy, M. J., Murugesan, G. P., Arora, M., Jain,
934 S. K., Ojha, C. S. P., Harrison, S., and Bamber, J.: Challenges in understanding the variability
935 of the cryosphere in the Himalaya and its impact on regional water resources,
936 <https://doi.org/10.3389/frwa.2022.909246>, 2022.

937 Wagnon, P., Linda, A., Arnaud, Y., Kumar, R., Sharma, P., Vincent, C., Pottakkal, J. G.,
938 Berthier, E., Ramanathan, A., Hasnain, S. I., and Chevallier, P.: Four years of mass balance
939 on Chhota Shigri Glacier, Himachal Pradesh, India, a new benchmark glacier in the western
940 Himalaya, *J. Glaciol.*, 53, 603–611, <https://doi.org/10.3189/002214307784409306>, 2007.

941 Wagnon, P., Brun, F., Khadka, A., Berthier, E., Shrestha, D., Vincent, C., Arnaud, Y., Six,
942 D., Dehecq, A., Ménégoz, M., and Jomelli, V.: Reanalysing the 2007–19 glaciological mass-
943 balance series of Mera Glacier, Nepal, Central Himalaya, using geodetic mass balance,
944 *Journal of Glaciology*, 67, 117–125, <https://doi.org/10.1017/jog.2020.88>, 2021.

945 Yao, J., Chen, Y., Guan, X., Zhao, Y., Chen, J., and Mao, W.: Recent climate and
946 hydrological changes in a mountain–basin system in Xinjiang, China, *Earth-Science*
947 *Reviews*, 226, 103957, <https://doi.org/10.1016/j.earscirev.2022.103957>, 2022.

948 Zemp, M., Thibert, E., Huss, M., Stumm, D., Rolstad Denby, C., Nuth, C., Nussbaumer, S.
949 U., Moholdt, G., Mercer, A., Mayer, C., Joerg, P. C., Jansson, P., Hynek, B., Fischer, A.,
950 Escher-Vetter, H., Elvehøy, H., and Andreassen, L. M.: Reanalysing glacier mass balance
951 measurement series, *The Cryosphere*, 7, 1227–1245, <https://doi.org/10.5194/tc-7-1227-2013>,
952 2013.

953 Zemp, M., Frey, H., Gärtner-Roer, I., Nussbaumer, S. U., Hoelzle, M., Paul, F., Haeberli, W.,
954 Denzinger, F., Ahlstrøm, A. P., Anderson, B., Bajracharya, S., Baroni, C., Braun, L. N.,

955 Cáceres, B. E., Casassa, G., Cobos, G., Dávila, L. R., Granados, H. D., Demuth, M. N.,
956 Espizua, L., Fischer, A., Fujita, K., Gadek, B., Ghazanfar, A., Hagen, J. O., Holmlund, P.,
957 Karimi, N., Li, Z., Pelto, M., Pitte, P., Popovnin, V. V., Portocarrero, C. A., Prinz, R.,
958 Sangewar, C. V., Severskiy, I., Sigurdsson, O., Soruco, A., Usubaliev, R., and Vincent, C.:
959 Historically unprecedented global glacier decline in the early 21st century, *Journal of*
960 *Glaciology*, 61, 745–762, <https://doi.org/10.3189/2015JoG15J017>, 2015.

961 Zemp, M., Huss, M., Thibert, E., Eckert, N., McNabb, R., Huber, J., Barandun, M.,
962 Machguth, H., Nussbaumer, S. U., Gärtner-Roer, I., Thomson, L., Paul, F., Maussion, F.,
963 Kutuzov, S., and Cogley, J. G.: Global glacier mass changes and their contributions to sea-
964 level rise from 1961 to 2016, *Nature*, 568, 382–386, [https://doi.org/10.1038/s41586-019-](https://doi.org/10.1038/s41586-019-1071-0)
965 [1071-0](https://doi.org/10.1038/s41586-019-1071-0), 2019.